N-63-4-3

Cruft Laboratory

Harvard University • Cambridge, Massachusetts

THEORETICAL AND EXPERIMENTAL STUDIES OF ANTENNAS AND ARRAYS IN A PARALLEL-PLATE REGION

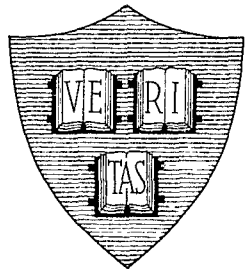

By

B. Rama Rao

October 5, 1962

Scientific Report No. 15 (Series 2)
Contract AF19(604)-4118 Project 5635, Task 563502
AFCRL-63-90

Prepared for
Electronics Research Directorate
Air Force Cambridge Research Laboratories
Office of Aerospace Research
United States Air Force • Bedford, Massachusetts

AFCRL-63-90

THEORETICAL AND EXPERIMENTAL STUDIES OF ANTENNAS AND ARRAYS IN A PARALLEL-PLATE REGION

by

B. Rama Rao

Division of Engineering and Applied Physics
Cruft Laboratory
Harvard University
Cambridge, Massachusetts

Contract AF19(604)-4118
Project 5635 - Task 563502
Scientific Report No. 15 (Series 2)
October 5, 1962

Prepared for

Electronics Research Directorate
Air Force Cambridge Research Laboratories
Office of Aerospace Research
United States Air Force
Bedford, Massachusetts

Requests for additional copies by Agencies of the Department of Defense, their contractors, and other Government agencies should be directed to the:

ARMED SERVICES TECHNICAL INFORMATION AGENCY
ARLINGTON HALL STATION
ARLINGTON 12, VIRGINIA

Department of Defense contractors must be established for ASTIA services, or have their "need-to-know" certified by the cognizant military agency of their project or contract.

All other persons and organizations should apply to the:

U. S. DEPARTMENT OF COMMERCE
OFFICE OF TECHNICAL SERVICES
WASHINGTON 25, D. C.

SR15

THEORETICAL AND EXPERIMENTAL STUDIES OF ANTENNAS AND ARRAYS IN A PARALLEL-PLATE REGION

PART I - THE CURRENT DISTRIBUTION AND IMPEDANCE OF AN ANTENNA IN A PARALLEL-PLATE REGION

by

B. Rama Rao

ABSTRACT

The integral equation for the current on the antenna has been formulated using Green's theorem and a suitable Green's function based on the method of images; the resulting equation has been solved by expressing the current as a Fourier series in terms of waveguide modes. It has been shown that in the case of thick antennas the logarithmic term in the current, due to the idealized delta-function generator, makes a marked contribution over a significant length of the antenna and the so-called 'transition' region is much larger than for the free-space antenna. The admittance of the theoretical model can be brought into good agreement with the experimental results by subtracting out the infinite gap capacitance and replacing it by an empirical correction term to account for the input susceptance of the actual feeding gap. An anomaly in the behavior of the antenna at resonance, noticed by Lewin, can be avoided by assuming a complex propagation constant in the guide, due to small but finite losses in the image planes. Closed form expressions for the current and admittance have

been obtained and compared with experimental results. The general agreement is found to be good.

To avoid complications due to the feed-point singularity, the admittance has also been obtained by a variational method. There is good agreement with experimental results for antenna lengths in the range $0 < k_o h < 3.7$; but the theory deteriorates for higher values of $k_o h$.

Extensive experimental measurements have been made on the antenna and a description of the apparatus is included in the report.

1. INTRODUCTION

Much attention has been focused during recent years on obtaining mathematically rigorous solutions to a large variety of problems concerning antennas radiating in free space (1); depending on the complexity and nature of the problem the techniques employed range from rigorous Fourier-transform and Fourier-series solutions to the more approximate iterative and variational techniques. In most cases the theoretical results have been supported by comprehensive experimental investigations. In contrast, however, the general problem of determining the current distribution and driving-point impedance of antennas radiating into waveguides has received scant attention until quite recently. Most of the early investigations (2) were confined to obtaining the impedance of small, 'filamentary' antennas employing the emf method with an assumed current distribution on the antenna. The inherent inadequacy of such a method as compared to the more sophisticated integral equation method and its variational modification has been pointed out by King (1). In practice, it is also not permissible to lay such severe restrictions on the finite thickness and size of the antenna. Lewin (3,4) has lately given the problem a more careful mathematical treatment. In a recent paper (3), he has considered the radiation from a linear antenna in a parallel-plate region using a modal expansion method. The solutions he obtains for the current and input admittance are not in a closed form and cannot be evaluated numerically for comparison with experimental results. Furthermore, he has noticed certain anomalies concerning the behavior of the antenna near resonance which cannot be

explained physically; all of these aspects deserve further examination, both theoretically and experimentally. The main motivation for the present investigation, however, arose while considering the propagation of surface waves along an antenna array placed in a parallel-plate region; for treating this problem rigorously it was necessary to know the current distribution on the individual elements of the array and the mutual coupling between the elements. An exact solution to the simple problem of a single antenna in the parallel-plate region is a necessary prerequisite towards obtaining a better understanding of this more complicated problem.

In this report an integral equation technique has been employed to obtain the current distribution and admittance of the antenna. The mathematical procedure adopted here closely follows that used for solving the free-space antenna problem. Since these two cases are twin aspects of the general problem of antenna radiation, a comparison between them might prove to be instructive. Another attractive advantage of the integral equation method is that it can readily be extended, as outlined by King (1), for obtaining the current distribution on coupled antennas or in an array of antennas.

To facilitate experimental measurements the antenna was driven near its base by means of a coaxial line connected to one of the ground planes; this is in contrast to Lewin's case (3) where the antenna was driven at its center between two plates, but it was not a practically feasible scheme and had to be discarded. Other than this slight difference, the problem treated here and the one considered by Lewin are identical.

In Sec. 2 the integral equation for the current has been solved by expressing the current on the antenna as a Fourier series in terms of waveguide modes. Special attention has been paid to the following aspects of the problem: (1) the logarithmic singularity in the current and its effect on admittance, (2) the behavior of the antenna at resonance, (3) current on an infinitesimally thin antenna, (4) the charge distribution on the antenna, (5) the effect of assuming a filamentary kernel in the integral equation. Closed-form solutions for the current and admittance have been obtained and compared with the experimental results. The general agreement is very good.

While the Fourier-series method provides accurate solutions for the current distribution and conductance of the antenna, the susceptance values obtained from it are rather ambiguous owing to the infinite gap capacitance of the delta-function generator. In Sec. 3 the impedance of the antenna has been obtained by a variational technique using a suitable trial function for the current. The variational method ignores the singularity at the driving point and provides an approximate but continuous solution for the current distribution over the entire length of the antenna. The theoretical and experimental admittance values are in excellent agreement until $k_o h = 3.7$ but deteriorate rapidly thereafter.

Section 4 is devoted to experimental phase of the research. A description is given of the apparatus and experimental techniques used for determining the current distribution and admittance of the antenna.

2. FOURIER-SERIES SOLUTION

Formulation of the Problem

The antenna under consideration is the center conductor of the coaxial cable which extends inside the parallel-plate region and has its upper end connected to the top plate. Fig. 1.1 shows the geometry of the idealized model driven by a delta-function generator. A cylindrical coordinate system (r, θ, z) is introduced and the axis of the antenna of radius a is made to coincide with the z axis. The two infinite, perfectly conducting image planes are situated at $z = 0$ and $z = h$. The antenna is assumed to be excited by a slice generator situated at $z = \pm \delta$. The equivalent structure obtained by considering successive reflections in the two planes is that of an infinitely long antenna fed by generators along the entire length spaced at intervals depending on the distance h between the two planes. Alternatively, the antenna may also be considered as an infinitely long collinear antenna array of half length h, placed end to end.

Because of angular symmetry, the only nonvanishing components of the field are E_z, E_r and H_θ. Since E_r vanishes at the two plates, the z component of the vector potential A_z satisfies the Neumann boundary condition

$$\frac{\partial A_z}{\partial z} = 0 \quad \text{at} \quad z = 0 \quad \text{and} \quad h. \tag{1.1}$$

The general equation satisfied by A_z at all points outside the conductors is

$$(\nabla^2 + k_o^2)\, A_z = 0 \tag{1.2}$$

where $k_o = 2\pi/\lambda$ is the wave number.

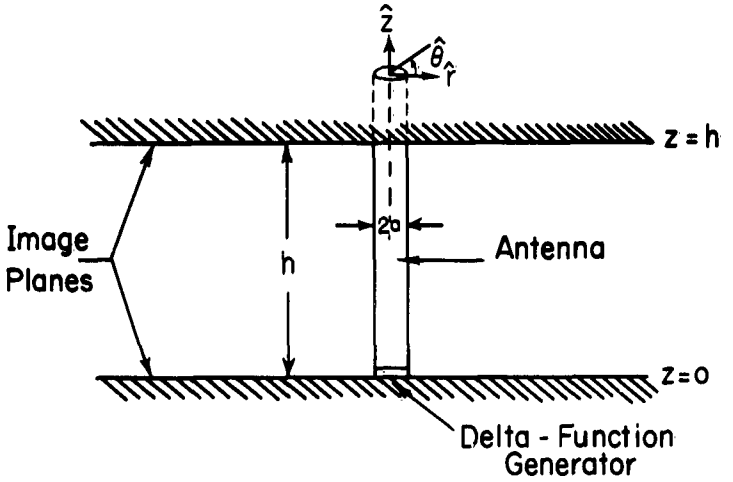

FIG. 1-1 Antenna in a Parallel-Plate Region Driven By Idealized Delta Function Generator

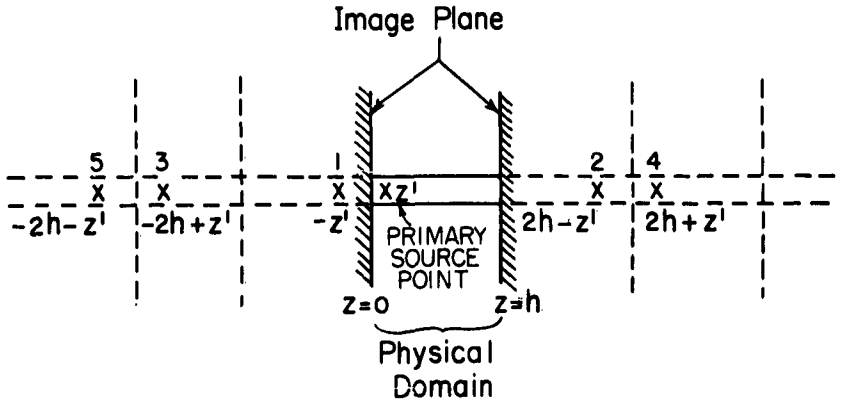

FIG. 1-2. Image Representation of Greens Function

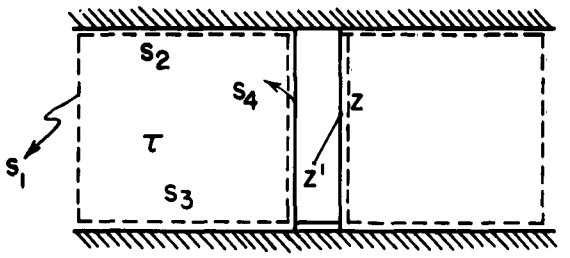

FIG. 1-3 Application of Greens Symmetric Theorem to Antenna Configuration.

The solution of this equation may be obtained by applying Green's symmetric theorem

$$\int_{\tau} \left[u\nabla^2 v - v\nabla^2 u \right] d\tau' = \int_{\Sigma} \left[u \frac{\partial v}{\partial n} - v \frac{\partial u}{\partial n} \right] d\sigma' \qquad (1.3)$$

with $u = A_z$ and $v = G$, where G is the Green's function satisfying an inhomogeneous wave equation with periodically distributed sources (see ensuing discussion)

$$\left[\nabla^2 + k_o^2 \right] G = - \sum_m - \delta (r - r_m') \qquad (1.4)$$

and the following boundary conditions:

(1) G is continuous except at $r = r_m'$ where it has a logarithmic singularity,

(2) G satisfies the radiation condition at $r \to \infty$ and the Neumann boundary condition $\frac{\partial G}{\partial z} = 0$ at $z = 0$ and h.

k_o is the free-space wave number; r and r_m' are the vector coordinates of the field and source points respectively; $\delta (r - r_m')$ is the three-dimensional Dirac delta function defined in the usual manner as

$$\delta (r - r_m') = 0 \quad r \neq r_m'$$

$$\int_{\tau} \delta (r - r_m') \, d\tau = 1 \quad \text{if } \tau \text{ includes } r_m'$$

$$= 0 \quad \text{if } \tau \text{ excludes } r_m' .$$

Image Representation of the Green's Function

The appropriate Green's function for the problem can be constructed by using the principle of images (see Fig. 1.2). Let the primary source point

The solution of this equation may be obtained by applying Green's symmetric theorem

$$\int_{\tau} \left[u\nabla^2 v - v\nabla^2 u \right] d\tau' = \int_{\Sigma} \left[u \frac{\partial v}{\partial n} - v \frac{\partial u}{\partial n} \right] d\sigma' \qquad (1.3)$$

with $u = A_z$ and $v = G$, where G is the Green's function satisfying an inhomogeneous wave equation with periodically distributed sources (see ensuing discussion)

$$\left[\nabla^2 + k_o^2 \right] G = - \sum_m - \delta (r - r_m') \qquad (1.4)$$

and the following boundary conditions:

(1) G is continuous except at $r = r_m'$ where it has a logarithmic singularity,

(2) G satisfies the radiation condition at $r \to \infty$ and the Neumann boundary condition $\frac{\partial G}{\partial z} = 0$ at $z = 0$ and h.

k_o is the free-space wave number; r and r_m' are the vector coordinates of the field and source points respectively; $\delta (r - r_m')$ is the three-dimensional Dirac delta function defined in the usual manner as

$$\delta (r - r_m') = 0 \quad r \neq r_m'$$

$$\int_{\tau} \delta (r - r_m') \, d\tau = 1 \quad \text{if } \tau \text{ includes } r_m'$$

$$= 0 \quad \text{if } \tau \text{ excludes } r_m' .$$

Image Representation of the Green's Function

The appropriate Green's function for the problem can be constructed by using the principle of images (see Fig. 1.2). Let the primary source point

be situated at z'. With consideration of its successive reflections in the two planes an infinite series of image sources is obtained. These are located at 2mh-z' where m = 0, ± 1, ± 2... and at 2mh + z' where m = ± 1, ± 2,... as shown in Fig. 1.2. The resultant effect of all these image sources is such that G satisfies the Neumann boundary condition $\partial G/\partial z = 0$ at z = 0 and h.

In view of the above discussion and in analogy with free-space antenna theory, a suitable Green's function satisfying all the boundary conditions mentioned in Eq. 1.4 is

$$G = \sum_{m=-\infty}^{\infty} \frac{e^{-jk_o R_m}}{4\pi R_m} \tag{1.5}$$

where $R_m = |r - r_m'|$ denotes the vector distance between the field and source points.

Now consider Eqs. 1.2 and 1.4 and apply Green's symmetric theorem to a pill-box shaped surface of the form shown in Fig. 1.3. It follows from Eq. 1.3 that

$$\int_\tau \left[G(\nabla^2 A_z + k_o^2 A_z) - A_z(\nabla^2 G + k_o^2 G) \right] d\tau'$$

$$= \int_{S_1+S_2+S_3+S_4} \left(G\, \partial A_z/\partial n - A_z \frac{\partial G}{\partial n} \right) d\sigma' \tag{1.6}$$

where S_1 is the outer surface of the pill-box, S_2 and S_3 are the top and bottom surfaces and S_4 the circumference of the antenna. As S_1 recedes to infinity, the integral over S_1 reduces to zero since both A_z and G vanish at infinity due

to the radiation condition. Also the integrals over S_2 and S_3 contribute nothing since both $\partial A_z/\partial n$ and $\frac{\partial G}{\partial n}$ vanish on the image plates.

Furthermore, since $A_r = A_\theta = \partial A/\partial\theta = 0$, and since the method of excitation is such that only the z component K_z of the current exists on the antenna, A_z has to satisfy the following boundary condition on the surface S_4 of the antenna.

$$\left(\frac{\partial A_z}{\partial r}\right)_{r=a} = \frac{K_z}{\nu} \qquad (1.7)$$

where K_z is the current density on the surface of the antenna.

Thus, of the four functions in equation 1.6 only $\partial A_z/\partial z$ is discontinuous across S_4. Hence,

$$\int_\tau A_z \ \delta(r - r_o')\, d\tau' = \frac{1}{\nu} \int_{S_4} K_z(z')\, G\, d\sigma' \qquad (1.8)$$

where r_o' refers to the vector coordinates of the primary source point. With $I(z') = 2\pi a\, K_z(z')$, Eq. 1.8 becomes

$$A_z(r) = \frac{1}{\nu}\int_o^h I_z(z')\, dz' \int_o^{2\pi} G\, \frac{d\phi}{2\pi} \qquad (1.9)$$

where $\phi = \theta' - \theta$ and G is given by 1.5.

From antenna theory the distance R_m in the kernel is given by

$$R_m = \left[(z \pm z' - 2mh)^2 + (2a \sin \phi/2)^2 \right]^{1/2}. \qquad (1.10)$$

The substitution of 1.5 and 1.10 in 1.9 leads to

$$A_z(r) = \frac{1}{4\pi\nu}\int_0^h I_z(z')\,dz' \int_0^{2\pi} \left\{ \sum_{m=-\infty}^{\infty} \frac{e^{-jk_o\left[(z-z'-2mh)^2 + (2a\sin\phi/2)^2\right]^{1/2}}}{\left[(z-z'-2mh)^2 + (2a\sin\phi/2)^2\right]^{1/2}} \right.$$

$$\left. + \sum_{m=-\infty}^{\infty} \frac{e^{-jk_o\left[(z+z'-2mh)^2 + (2a\sin\phi/2)^2\right]^{1/2}}}{\left[(z+z'-2mh)^2 + (2a\sin\phi/2)^2\right]^{1/2}} \right\} d\phi/2\pi \quad . \qquad (1.11)$$

The series occurring above can be converted into a more convenient form by using Poisson's summation formula given by

$$\sum_{m=-\infty}^{\infty} f(am) = 1/a \sum_{m=-\infty}^{\infty} F(2m\pi/a) \qquad (1.12)$$

where $F(\omega)$ is the Fourier transform of $f(t)$ and is defined by

$$f(t) = \frac{1}{2\pi}\int_{-\infty}^{+\infty} e^{-j\omega t} F(\omega)\,d\omega \quad . \qquad (1.13)$$

The required Fourier transform in this case is

$$\int_{-\infty}^{+\infty} e^{j\omega t} \exp\left\{ \frac{-jk_o\left[c^2 + (\xi - t)^2\right]^{1/2}}{\left[c^2 + (\xi - t)^2\right]^{1/2}} \right\}$$

$$= 2e^{j\omega\xi} K_o\left[c^2(\omega^2 - k_o^2)^{1/2}\right] \qquad (1.14)$$

where K_o is the modified Bessel function of the second kind. With 1.14 and 1.12 in 1.11 it follows that

$$\sum_{m=-\infty}^{+\infty} \frac{e^{-jk_o\left[(z - z' - 2mh)^2 + (2a\sin \phi'/2)^2\right]^{1/2}}}{\left[(z - z' - 2mh)^2 + (2a\sin \phi/2)^2\right]^{1/2}}$$

$$= \sum_{m=-\infty}^{\infty} \frac{1}{h} e^{j\frac{m\pi}{h}(z-z')} K_o\left\{(2a\sin\frac{\phi}{2})^2\left[(\frac{m\pi}{h})^2 - k_o^2\right]\right\} \quad . \quad (1.15)$$

Similarly,

$$\sum_{m=-\infty}^{\infty} \frac{e^{-jk_o\left[(z + z' - 2mh)^2 + (2a\sin \phi'/2)^2\right]^{1/2}}}{\left[(z + z' - 2mh)^2 + (2a\sin \phi'/2)^2\right]^{1/2}}$$

$$= \sum_{m=-\infty}^{\infty} \frac{1}{h} e^{j\frac{m\pi}{h}(z + z')} K_o\left\{(2a\sin\frac{\phi}{2})^2\left[\left(\frac{m\pi}{h}\right)^2 - k_o^2\right]\right\} \cdot \quad (1.16)$$

In the above equations $\sqrt{\left(\frac{m\pi}{h}\right)^2 - k_o^2} = \Gamma_m$ is easily recognized to be the mode propagation constant in the parallel-plate guide.

It is now possible to add (1.15) and (1.16) and combine the terms symmetrically with respect to $m = 0$. With this result in 1.11 and the substitution of 2θ for ϕ, the following result is obtained

$$A_z(r) = \frac{1}{2\pi\nu}\int_o^h I(z')\,dz' \cdot \frac{1}{\pi h}\sum_{m=-\infty}^{\infty}\left\{\int_o^{\pi} K_o(2k_o a\,\gamma_m \sin\theta)\,d\theta\right\}$$

$$\cos\frac{m\pi z}{h} \quad \cos\frac{m\pi z'}{h} \qquad (1.17)$$

where

$$\gamma_m = \sqrt{\left(\frac{m\pi}{k_o h}\right)^2 - 1} \quad . \qquad (1.18)$$

The tangential component of the electric field on the surface of the antenna is given by

$$\left(E_z\right)_{r=a} = \frac{-j\omega}{k_o^2} \left[\frac{\partial^2 A_z}{\partial z^2} + k_o^2 A_z\right]_{r=a} \quad . \qquad (1.19)$$

With Eq. 1.17 it follows that

$$\left(E_z\right)_{r=a} = -j\zeta_o \frac{k_o}{2\pi^2 h} \int_o^h I_z(z')\,dz' \sum_{m=-\infty}^{\infty} \int_o^{\pi} \left[K_o(2k_o a \gamma_m \sin\theta)d\theta\right] \left\{1 - (m\pi/k_o h)^2\right\} \cos\frac{m\pi z}{h} \cos\frac{m\pi z'}{h} \quad . \qquad (1.20)$$

The electric field along the surface of the antenna $\left[E_z\right]_{r=a}$ must be equal to $Z^i I(z)$ $(z \neq 0)$ where Z^i is the internal impedance. The driving voltage V_o of the slice generator is given by

$$-V_o = \lim_{\delta \to 0} \int_{-\delta}^{\delta} \left(E_z^e\right)_{r=a} dz \qquad (1.21)$$

where $\left(E_z^e\right)_{r=a}$ is the impressed field maintained across a thin slice 2δ on the surface of the conductor. From the nature of Eq. 1.21, it is seen that at $z = 0$, $\left(E_z\right)_{r=a}$ can be expressed in terms of the Dirac delta function as

$$(E_z^e)_{r=a} = - V_o \delta(z)$$

Hence, the electric field at any point along the antenna is

$$(E_z)_{r=a} = Z^i I(z) - V_o \delta(z) \quad 0 < z < h$$

For a perfectly conducting antenna $Z^i = 0$ and

$$(E_z)_{r=a} = - V_o \delta(z) \tag{1.22}$$

From 1.22 and 1.20

$$V_o \delta(z) = j\zeta_o \int_o^h K(z, z') I(z') dz' \tag{1.23}$$

where the kernel of the integral equation $K(z, z')$ is given by

$$K(z, z') = \frac{k_o}{2\pi^2 h} \left[\int_o^\pi K_o(j2k_o a \sin\theta) \, d\theta - 2 \sum_{m=1}^{\infty} \int_o^\pi \left\{ K_o(2k_o a \gamma_m \sin\theta) \right\} d\theta \left[\left(\frac{m\pi}{k_o h} \right)^2 - 1 \right] \cos\frac{m\pi z}{h} \cos\frac{m\pi z'}{h} \right]. \tag{1.24}$$

The integrals appearing in 1.24 can now be evaluated by means of the appropriate integral representation for the Bessel functions. The formulas used in the derivation below are all obtained from Magnus and Oberhettinger (5), which will hereafterwards be briefly referred to as (M and O).

Consider the first integral

$$P = \int_0^{\pi} K_o(ak_o a\gamma_m \sin\theta)\, d\theta = \int_0^{\pi} K_o(c_m \sin\theta)\, d\theta \qquad (1.25)$$

where

$$c_m = 2k_o a\gamma_m .$$

The integral representation for the K_o function is given by M and O (5) page 27 as

$$K_o(ax) = \int_0^{\infty} \frac{\cos x t}{\sqrt{a^2 + t^2}}\, dt \quad (a,\ x \text{ real and positive}) .$$

With this result it follows that

$$P = \int_0^{\pi} \int_0^{\infty} \frac{\cos\left[t \sin\theta\right]}{\sqrt{c_m^2 + t^2}}\, dt\, d\theta = \int_0^{\infty} \frac{dt}{\sqrt{c_m^2 + t^2}} \int_0^{\pi} \cos\left[t \sin\theta\right] d\theta$$

$$= \pi \int_0^{\infty} \frac{J_o(t)}{\sqrt{c_m^2 + t^2}}\, dt . \qquad (1.26)$$

Use is now made of Watson's formula (5) [M and O p. 30]

$$I_{\nu/2}\left(\tfrac{1}{2} ax\right) K_{\nu/2}\left(\tfrac{1}{2} ax\right) = \int_0^{\infty} \frac{J_\nu(at)}{\left(t^2 + x^2\right)^{1/2}}\, dt$$

$$(\mathrm{Re}\ \nu > -1,\ a \text{ real and positive},\ |\arg x| < \pi/2) .$$

With $\nu = 0$ in the above equation and with the substitution of this result in 1.26 , it follows that

$$P = \int_0^{\pi} K_o (2k_o a \gamma_m \sin\theta)\, d\theta = \pi I_o (k_o a\gamma_m) K_o (k_o a\gamma_m) \qquad (1.27)$$

where I_o and K_o are the modified Bessel functions of the first and second kind.

For imaginary arguments the identities $I_o(jz) = J_o(z)$ and $K_o(jz) = -j\frac{\pi}{2} H_o^{(2)}(z)$ apply, where $J_o(z)$ is the Bessel function of the first kind and $H_o^{(2)}(z)$ is the Hankel function of the second kind. With $m = 0$ in 1.27 and with these several identities it follows that

$$\int_0^{\pi} K_o (j2k_o a \sin\theta)\, d\theta = -\frac{j\pi}{2} \int_0^{\pi} H_o^{(2)} (k_o a \sin\theta)\, d\theta$$

$$= \frac{-j\pi^2}{2} J_o (k_o a) H_o^{(2)} (k_o a) . \qquad (1.28)$$

(See Appendix I for rigorous derivation of this formula).

The substitution of 1.27 and 1.28 in 1.24 leads to

$$K(z, z') = \frac{-k_o}{2\pi h} \left\{ j\frac{\pi}{2} J_o (k_o a) H_o^{(2)} (k_o a) + 2\sum_{m=1}^{\infty} I_o (k_o a\gamma_m) K_o (k_o a\gamma_m) \left[\left(\frac{m\pi}{k_o h}\right)^2 - 1\right]^{-\frac{1}{2}} \frac{\cos m\pi z}{h} \frac{\cos m\pi z'}{h} \right\}$$

$$\text{for } 0 < k_o h < \pi . \qquad (1.29)$$

When the separation of the parallel plate exceeds a half-wavelength, that is when $\pi/k_o h < 1$, the term corresponding to $m = 1$ has to be modified to account for the propagation of the first higher-order mode in the parallel-plate medium. The corresponding expression for the kernel is

$$K(z,z') = \frac{-k_o}{2\pi h}\left\{ j\frac{\pi}{2} J_o(k_o a) H_o^{(2)}(k_o a) \right.$$

$$+ 2\frac{j\pi}{2}\left[1-(\pi/k_o h)^2\right] J_o\left[k_o a\sqrt{1-(\pi/k_o h)^2}\right] H_o^{(2)}\left[k_o a\sqrt{1-(\pi/k_o h)^2}\right] \frac{\cos\pi z}{h} \cdot \frac{\cos\pi z}{h}$$

$$\left. + 2\sum_{m=2}^{\infty} I_o(k_o a\gamma_m) K_o(k_o a\gamma_m)\left[\left(\frac{m\pi}{k_o h}\right)^2 - 1\right] \frac{\cos m\pi z}{h} \cdot \frac{\cos\pi z'}{h} \right\}$$

$$\text{for } \pi < k_o h < 2\pi , \qquad (1.30)$$

Fourier-Series Solution

To obtain the Fourier-series solution for the current distribution along the antenna, consider first Eq. 1.23.

$$V_o \cdot \delta(Z) = j\zeta_o \int_o^h K(z,z')\ I(z')\, dz'$$

where the kernel from Eq. 1.29 may be written as

$$K(z,z') = a_o + 2\sum_{m=1}^{\infty} a_m \cos m\pi z/h \cdot \cos m\pi z'/h \ . \qquad (1.31)$$

In Eq. 1.31

$$a_o = -\frac{k_o}{2\pi h} \cdot \frac{j\pi}{2} \cdot J_o(k_o a) \cdot H_o^{(2)}(k_o a)$$

$$\text{and } a_m = -\frac{k_o}{2\pi h}\left[\left(\frac{m\pi}{k_o h}\right)^2 - 1\right] I_o(k_o a\gamma_m) \cdot K_o(k_o a\gamma_m) \ . \qquad (1.32)$$

The current on the antenna may now be expressed in terms of the Fourier series

$$I(z) = I_o + 2 \sum_{m=1}^{\infty} I_m \cos m\pi/h \quad . \tag{1.33}$$

After the substitution of 1.33 in 1.31 the integration may be performed to obtain

$$I_m = V_o / j\zeta_o h^2 a_m \quad .$$

The current distribution on the antenna is then given by

$$I(z) = I''(z) + jI'(z) = \frac{V_o}{j\zeta_o h^2} \left\{ \frac{1}{a_o} + 2 \sum_{m=1}^{\infty} \frac{\cos m\pi z/h}{a_m} \right\}$$

$$= \frac{jV_o}{60k_o h} \left\{ \frac{1}{j\frac{\pi}{2} J_o(k_o a) H_o^{(2)}(k_o a)} + 2 \sum_{m=1}^{\infty} \frac{\cos m\pi z/h}{\gamma_m^2 I_o(k_o a\gamma_m) K_o(k_o a\gamma_m)} \right\} \tag{1.34}$$

where I'' is the component of the current in phase and I' is the component of the current in phase quadrature with the driving voltage and the admittance $Y = \left(\frac{Y}{V}\right)_{z=0}$ is

$$Y = \frac{j}{60k_o h} \left\{ \frac{1}{j\frac{\pi}{2} J_o(k_o a) H_o^{(2)}(k_o a)} + 2 \sum_{m=1}^{\infty} \frac{1}{\gamma_m^2 I_o(k_o a\gamma_m) K_o(k_o a\gamma_m)} \right\}$$

$$\text{when } 0 < k_o h < \pi \quad . \tag{1.35}$$

When the plate separation is greater than a half-wavelength

$$Y = \frac{j}{60 k_o h} \left\{ \frac{1}{j\frac{\pi}{2} J_o(k_o a) H_o^{(2)}(k_o a)} \right.$$

$$+ \frac{2}{j\frac{\pi}{2}\left[1 - \left(\frac{\pi}{k_o h}\right)^2\right] J_o\left(k_o a\sqrt{1 - \left(\frac{\pi}{k_o h}\right)^2}\right) H_o^{(2)}\left(k_o a\sqrt{1 - (\pi/k_o h)^2}\right)}$$

$$\left. + 2\sum_{m=2}^{\infty} \frac{2}{\gamma_m^2 I_o(k_o a\gamma_m) K_o(k_o a\gamma_m)} \right\}. \qquad (1.36)$$

From 1.35 it is seen that the conductance of the antenna is due only to the primary TEM wave corresponding to m = 0, whereas all the evanescent higher modes contribute only to the susceptance. When the plate separation is increased beyond a half-wavelength, the first higher-order mode m = 1 starts propagating and introduces a conductance term, as can be seen from 1.36. Because of this coupling between the two modes, the conductance of the antenna is now larger, signifying increased radiation. As the plate separation increases further, the higher-order modes cause a periodic increase in the antenna conductance.

Closed-Form Solutions for the Current Distribution

For sufficiently large values of m

$$\gamma_m = \sqrt{(m\pi/k_o h)^2 - 1} \approx m\pi/k_o h$$

and

$$k_o a\gamma_m \simeq m\pi \frac{a}{h}.$$

Therefore, for the higher-order terms the I_o and K_o functions may be replaced by their asymptotic values given by

$$I_o(x) \sim e^{x}/(2\pi x)^{1/2} \text{ and } K_o(x) \sim (\pi/2x)^{1/2} e^{-x} \text{ for large } x. \quad (1.37)$$

With these results it follows that

$$\gamma_m^2 I_o(k_o a\gamma_m) K_o(k_o a\gamma_m) \simeq \frac{\gamma_m}{2k_o a} \simeq \frac{m\pi}{2(k_o a)(k_o h)}. \quad (1.38)$$

To obtain closed-form expressions for the current the series in 1.34 can be truncated at $M \simeq h/\pi a$ and 1.36 can be substituted in the coefficients of the higher-order terms.

The current is then given by

$$I(z) = \frac{jV}{60k_o h}\left[\frac{1}{j\frac{\pi}{2} J_o(k_o a)H_o^{(2)}(k_o a)} + 2\sum_{m=1}^{M} \frac{\cos m\pi z/h}{\gamma_m^2 I_o(k_o a\gamma_m)K_o(k_o a\gamma_m)} + \frac{4(k_o a)\cdot(k_o h)}{\pi} \sum_{m=M}^{\infty} \frac{\cos m\pi z/h}{m}\right]. \quad (1.39)$$

The series in the last term of the right-hand side can be evaluated by means of the summation formula

$$\sum_{m=1}^{\infty} \frac{\cos m\pi z/h}{m} = -\ln\left[2\sin\frac{\pi}{2} z/h\right]. \quad (1.40)$$

With this formula in 1.39 the current distribution is given by

$$I(z) = \frac{jV}{60k_o h}\left\{\frac{1}{j\frac{\pi}{2} J_o(k_o a)\cdot H_o^{(2)}(k_o a)}\right.$$

$$+ 2 \sum_{m=1}^{M} \left[\frac{1}{\gamma_m^2 I_o(k_o a \gamma_m) . K_o(k_o a \gamma_m)} - \frac{2(k_o a).(k_o h)}{\pi} . \frac{1}{m} \right] \frac{\cos m\pi z}{h}$$

$$- 4/\pi \ (k_o a).(k_o h). \ln\left\{ 2 \sin (\pi z/2h) \right\}$$

$$\text{for } 0 < k_o h < \pi . \qquad (1.41)$$

In Fig. 1.5 the in-phase component I" and the phase-quadrature component I' of the current calculated from Eq. 1.41 for an antenna with $a/\lambda = 0.01058$ and $k_o h = \pi/2$ ($h = \lambda/4$) with M = 10 have been plotted. The in-phase component I", which is contributed only by the principal radiating TEM wave, is found to be constant over the entire length of the antenna; it makes a significant contribution to the current distribution. The phase-quadrature component I' is contributed by the evanescent higher-order modes; it involves the logarithmic term, and hence has a singularity near the driving point giving rise to an infinite gap susceptance; this aspect will be discussed in greater detail later. The logarithmic term actually represents the current charging the adjacent knife edges (with infinite capacitance) of the idealized delta-function generator. I' makes only a minor contribution near the end, where the behavior of the current distribution is determined mainly by I". The current amplitude $I'_z = \sqrt{I'^2_z + I''^2_z}$ therefore tends to flatten off at the end of the antenna as can be seen from Fig. 1.6.

The current distribution for antenna lengths in the range $\pi < k_o h < 2\pi$ is given by

$$I(z) = \frac{jV}{60k_o h} \left\{ \frac{1}{j\frac{\pi}{2} J_o(k_o a).H_o^{(2)}(k_o a)} \right.$$

$$+ 2\cos\frac{\pi z}{h} \left[\frac{1}{j\frac{\pi}{2}\left[\sqrt{1-(\pi/k_o h)^2}\right] J_o\left[\sqrt{1-(\pi/k_o h)^2}\right] H_o^{(2)}\left[\sqrt{1-(\pi/k_o h)^2}\right]} - \frac{2(k_o a)(k_o h)}{\pi} \right]$$

$$+ 2\sum_{m=2}^{M} \left(\frac{1}{\gamma_m^2 I_o(k_o a\gamma_m).K_o(k_o a\gamma_m)} - \frac{2(k_o a).(k_o h)}{\pi} \cdot \frac{1}{m} \right) \cdot \cos\frac{m\pi z}{h}$$

$$\left. - \frac{4(k_o a).(k_o h)}{\pi} \ln\left[2\sin(\pi z/2h)\right] \right\} \quad . \qquad (1.42)$$

In Fig. 1.8 the theoretical values (with M = 10) of I' and I'' for an antenna with $k_o h = 4.7124$ ($h = 3/4\lambda$), $a/\lambda = 0.01058$ have been plotted. Now the contribution to the in-phase component I'' comes from both the TEM wave and the first-order mode (m = 1). Since the first-order mode has a cosinusoidal dependence on length, the component I'' no longer is a constant as in the case of the quarter-wavelength antenna ($k_o h = \pi/2$). It has a slightly higher amplitude near the driving point than at the end.

The I' component again shows a logarithmic rise near the driving point; it has a minimum at $k_o z = 1.6$ but once again rises to a maximum near the end.

Numerical Accuracy of Calculations

The term M at which the series can be truncated is roughly given by $h/\pi a$ and depends on the thickness and height of the antenna. For shorter and thicker antennas fewer terms are required. In practice, however, the number of terms actually needed depends entirely on the desired numerical tolerance. For the case of the experimental antenna with $k_o a = 0.0664$ and with $k_o h$ ranging from 0.5 to 6.1 a summation of the first ten terms was found quite adequate to obtain the required degree of accuracy for comparison with experimental results. In Fig. 1.4 $1/I_o(k_o a\gamma_m) \cdot K_o(k_o a\gamma_m)$ has been plotted against its asymptotic equivalent $2k_o a\gamma_m$ for an antenna with $h = \lambda/4$ or $k_o h = \pi/2$ and $a/\lambda = 0.01058$ and also for $a/\lambda = 0.03175$. The term $M = h/\pi a$ in the two cases is approximately 8 and 3. It can be seen from the curves that the error in the truncation process is indeed very small.

Comparison with Experimental Results

In Fig. 1.6 and Fig. 1.7 the theoretical and experimental results for the amplitude of the current $|I| = \sqrt{I''^2 + I'^2}$ and the phase angle $\theta = \tan^{-1} I'/I''$ have been plotted. As can be seen there is excellent agreement between the two except near the driving point because of the logarithmic singularity.

In Figs. 1.8 and 1.9 the amplitude and phase of the current for an antenna with $k_o h = \frac{3\pi}{2}$ $(h = 3\lambda/4)$ and $a/\lambda = 0.01058$ have been calculated from Eq. 1.42 with M = 10, and compared with experimental results. Agreement is very good.

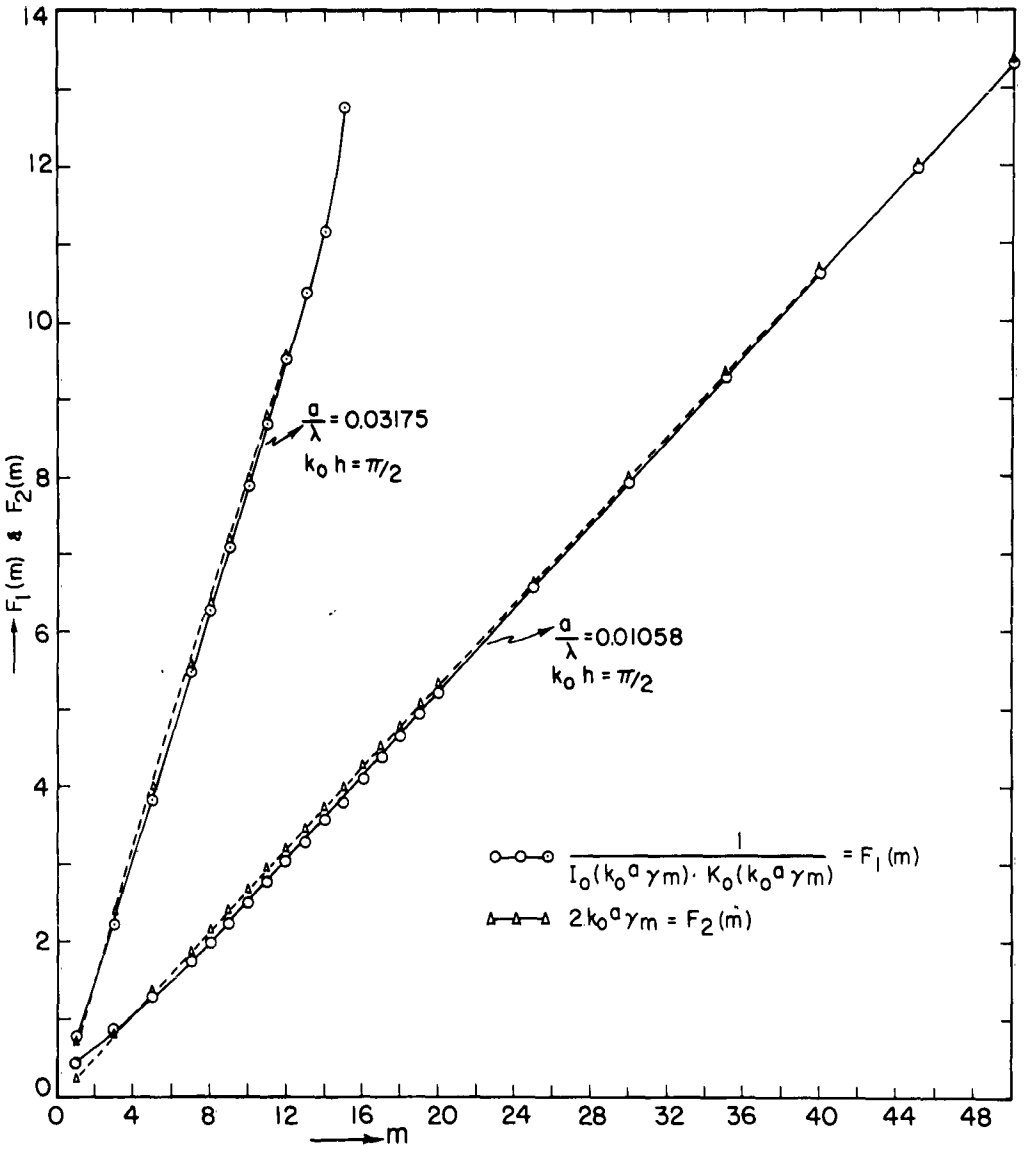

FIG 1-4 CURVES ILLUSTRATING THE VALIDITY OF THE TRUNCATION PROCESS.

$$\frac{1}{I_0(k_0 a\gamma m)\cdot K_0(k_0 a\gamma m)} = F_1(m)\ ;\quad 2k_0 a\gamma m = F_2(m)$$

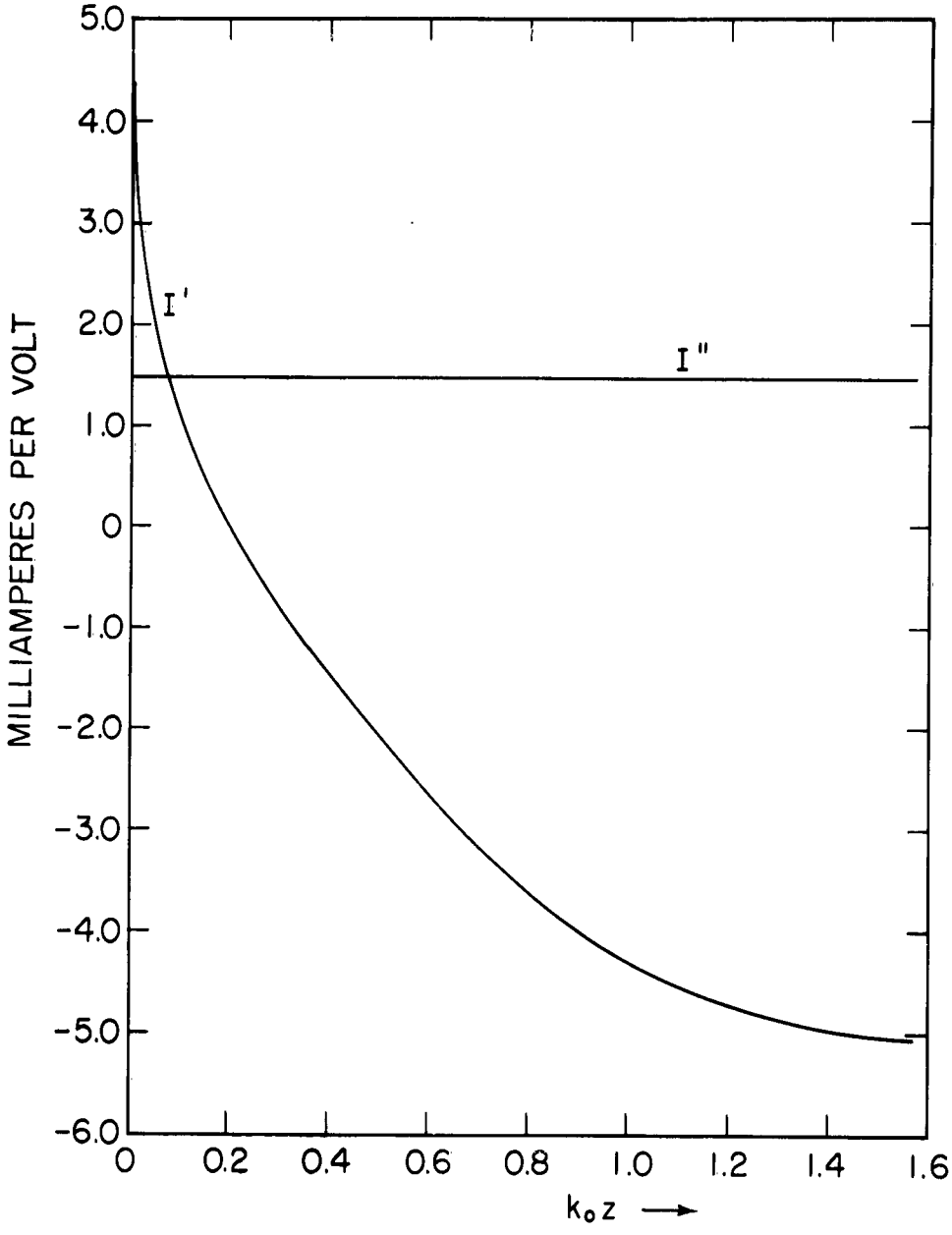

FIG. 1-5 THEORETICAL CURRENT DISTRIBUTION (FOURIER SERIES) $k_o h = \pi/2$; $k_o a = 0.0664$. $(a/\lambda = 0.0105)$; $M = 10$.

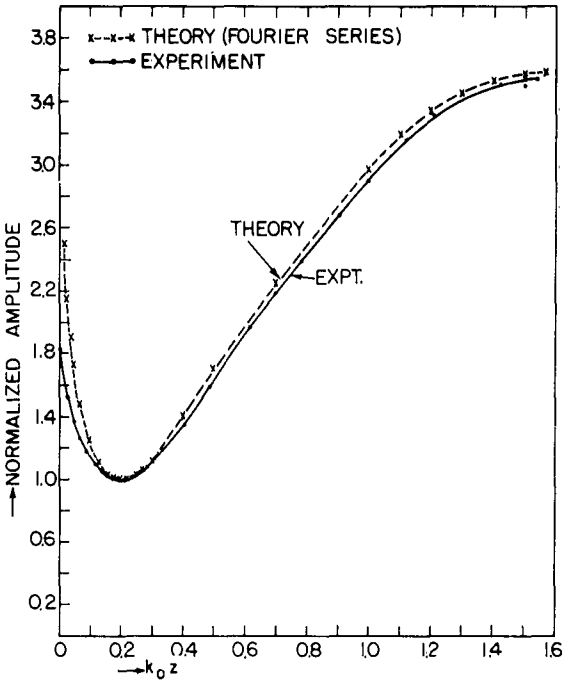

FIG. I-6 COMPARISON OF THEORETICAL AND EXPERIMENTALLY DETERMINED CURRENT DISTRIBUTION (AMPLITUDE) $k_0 h = \pi/2$; $a/\lambda = 0.0105$; M=10

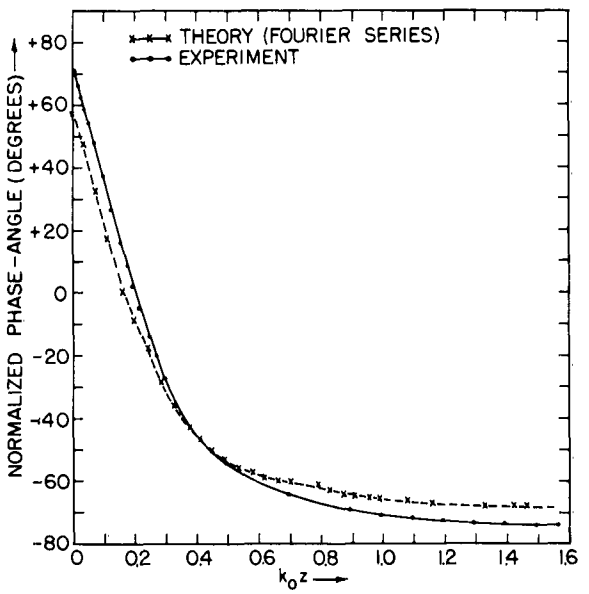

FIG. I-7 COMPARISON OF THEORETICAL AND EXPERIMENTALLY DETERMINED CURRENT DISTRIBUTION (PHASE). $k_0 h = \pi/2$; $a/\lambda = 0.0105$; M=10

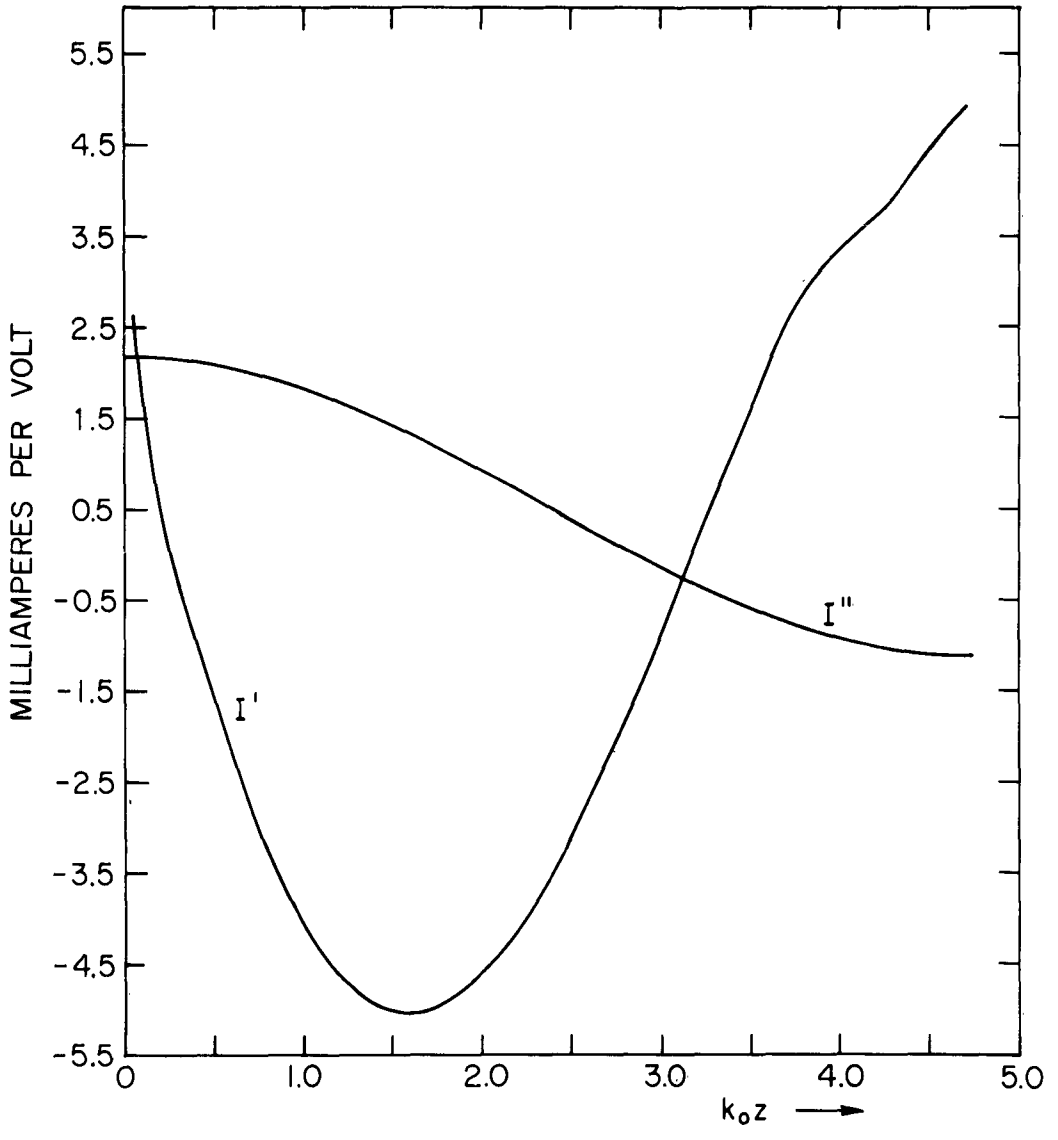

FIG. 1-8 THEORETICAL CURRENT DISTRIBUTION (FOURIER SERIES METHOD). $k_0 h = 3\pi/2$; $a/\lambda = 0.01058$; $M = 10$.

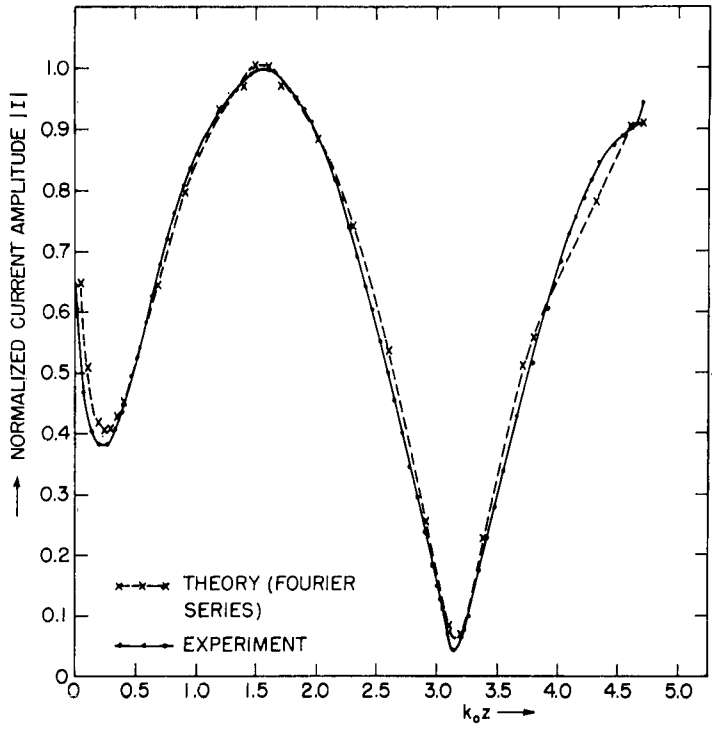

FIG. 1-9 COMPARISON OF THEORETICAL AND EXPERIMENTALLY DETERMINED CURRENT DISTRIBUTION (AMPLITUDE). $k_0h = 3\pi/2$; $a/\lambda = 0.0105$; $M = 10$.

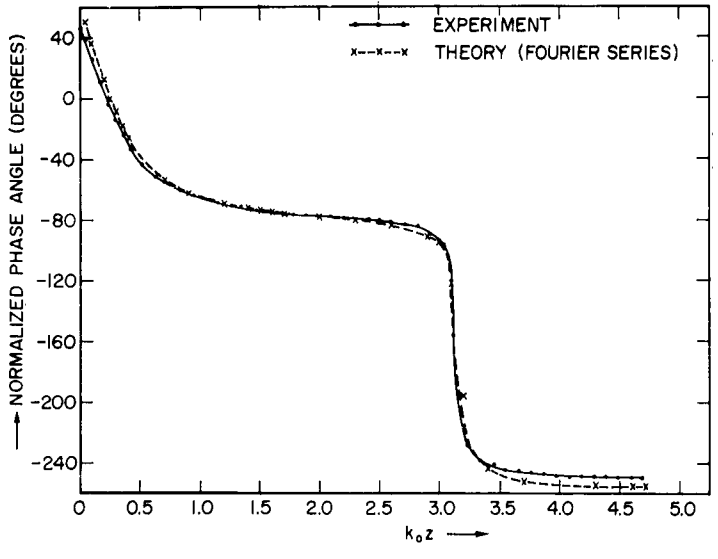

FIG. 1-10 COMPARISON OF THEORETICAL AND EXPERIMENTALLY DETERMINED CURRENT DISTRIBUTION (PHASE). $k_0h = 3\pi/2$; $a/\lambda = 0.01058$; $M = 10$.

Current Distribution and Admittance at Resonance

When the antenna is a half-wavelength, i.e., $k_o h = \pi$, the coefficient of the $\cos \pi z/h$ in Eq. 1.42 shows a singularity and needs close inspection. For small arguments $J_o(x) \sim 1$ and $H_o^{(2)}(x) \simeq 1 - j \frac{2}{\pi} \log(\beta x)$ where $\beta = \gamma - \log 2$ and γ = Euler's constant = 0.5772. With these identities used in the coefficient of the $\cos \pi z/h$ term in Eq. 1.36, the term containing the singularity may be denoted as follows:

$$P = \frac{2}{\left\{ j \frac{\pi}{2} + \gamma + \log\left(\frac{1}{2} k_o a \right) + \frac{1}{2} \log \nu \right\} \{\nu\}} \qquad (1.43)$$

where

$$\nu = 1 - (\pi / k_o h)^2 . \qquad (1.44)$$

When $k_o h = \pi$ ($\nu = 0$), $P = \infty$. This gives rise to an infinite current on the antenna. This, of course, is physically quite meaningless since the current on the antenna has always to be a finite quantity. A similar anomaly has also been reported by Lewin (3). To circumvent this difficulty it can be assumed that the parallel-plate region has a small but finite attenuation constant owing to losses in the two ground planes, so that k is now a

complex quantity with a small negative imaginary part $-j\alpha$, where α is the attenuation constant. This assumption is practically quite plausible since the image planes are never perfectly conducting. The complex wave number can be represented by $\bar{k} = \beta - j\alpha$, where $\beta = 2\pi/\lambda$.

For $\beta h = \pi$

$$\nu = 1 - \left\{ \frac{\pi}{(\beta - j\alpha)\, h} \right\}^2 = 1 - \left(\frac{\pi}{\pi - \frac{j\alpha\lambda}{2}} \right)^2$$

$$\simeq - \frac{j\alpha\lambda}{\pi} + \frac{\alpha^2\lambda^2}{4\pi^2} .$$

If the α^2 term is neglected, it follows that $\nu = - \frac{j\alpha\lambda}{\pi}$. (1.45)

Also $\bar{k}a \approx k_o a$. Substitution of these results in 1.43 gives $P = \tau/\alpha$ (1.46)

where $$\tau = \frac{2}{\left[j\pi/2 + \gamma + \log \left(\frac{1}{2} k_o a \right) + \frac{1}{2} \log \left(- \frac{j\alpha\lambda}{\pi} \right) \right]} .$$ (1.47)

Since the attenuation constant is generally a very small quantity, the $\cos \frac{\pi z}{h}$ term completely predominates over all other terms in 1.42 (except for the logarithmic term close to the driving point) and so the current on the half-wave resonant antenna becomes a pure cosine

$$I(z) = P \cos \pi z/h \qquad (1.48)$$

where P is given by 1.46.

This phenomenon has been confirmed experimentally. In Fig. 1.11 and Fig. 1.12 the experimentally observed amplitude and phase of the current on the antenna have been compared with the theoretical curve. There is close agreement between the two. The admittance of the half-wavelength antenna is

$$[Y]_{k_o h=\pi} = P = \tau / a \qquad . \qquad (1.49)$$

This is a very large quantity which is limited only by the small but finite attenuation constant of the parallel-plate region to the propagating waves. In Fig. 1.13 the theoretically calculated values for the conductance and susceptance of the antenna in the vicinity of resonance have been compared with the experimentally measured values. In Table 1-1 the measured values of conductance and susceptance of the antenna near resonance have been tabulated. From Fig. 1.13 and also Figs. 1.17 and 1.18 it can be seen that both the conductance and susceptance show a sharp, almost discontinuous rise near $k_o h = \pi$. The conductance particularly, as can be seen from Fig. 1.17, shows a sharp 'spike' when the antenna is nearly a half-wavelength

long. The conductance jumps from 2.29 millimhos at $k_o h = 3.07$ to 29.64 millimhos at $k_o h = 3.14$. Since the conductance is very sensitive to the antenna length near resonance, the experimental measurements had to be done with great care.

The antenna near resonance, therefore, behaves essentially like a short-circuited transmission line. The current is almost a pure cosine and its amplitude is very high. An examination of Figs. 1.11 and 1.12 shows that the current in the lower and upper halves of the antenna, while equal in magnitude, are 180^o out of phase and so their individual contributions to the field at distant points cancel out. This implies very little radiation loss or low radiation resistance and high conductance.

The same phenomenon repeats when $k_o h = 2\pi$, only this time the singularity is in the $m=2$ term and the current distribution is given by

$$I(z) \propto \cos 2\pi z/h \,. \tag{1.50}$$

In Fig. 1.14 the amplitude of the experimentally observed curve has been compared with theory to confirm the above result. The conductance again shows a sharp rise as can be seen from Fig. 1-17.

A more rigorous treatment of this phenomenon has recently been made by Tai Wu (6), without resorting to the expedient of a complex propagation constant.

$k_o h$	G[mhos x 10^3]	jB[mhos x 10^3]
2.41	1.13	+j8.02
2.63	1.00	+j10.83
2.71	1.12	+j11.76
2.83	1.06	+j14.72
2.89	1.16	+j17.75
2.93	1.22	+j20.18
2.99	1.28	+j26.65
3.02	1.16	+j31.22
3.05	1.87	+j36.92
3.07	2.29	+j44.14
3.11	4.18	+j72.77
3.14	29.64	+j189.25
3.20	18.10	-j79.02
3.30	12.68	-j27.87
3.46	6.98	-j9.81
3.68	4.20	-j3.62

TABLE 1-1. Measured Values of the Admittances Near Resonance ($a/\lambda = 0.01058$).

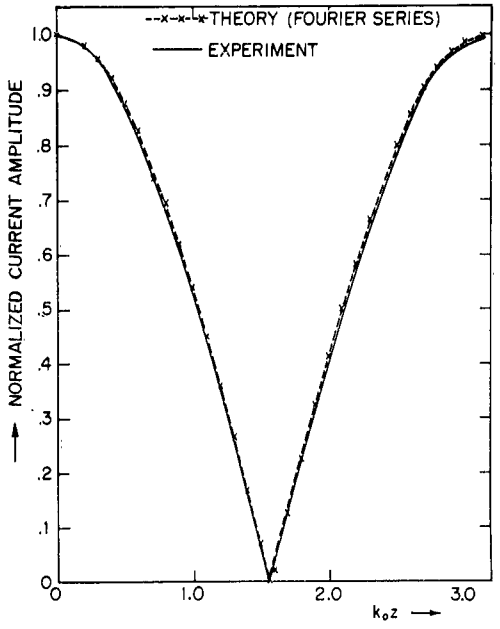

FIG. I-11 COMPARISON OF THEORETICAL AND EXPERIMENTALLY DETERMINED CURRENT DISTRIBUTION CURVES. (AMPLITUDE). $k_0h = \pi$; $a/\lambda = 0.0105$; M = 10.

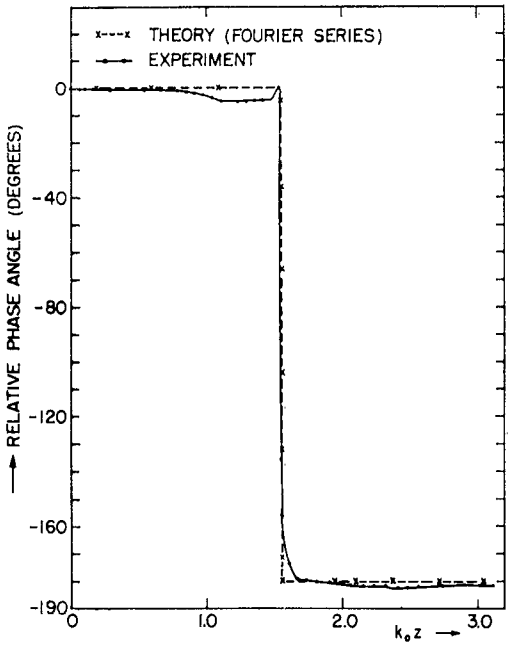

FIG. I-12 COMPARISON OF THEORETICAL AND EXPERIMENTALLY DETERMINED CURRENT DISTRIBUTION (PHASE). $k_0h = \pi$; $a/\lambda = 0.0105$

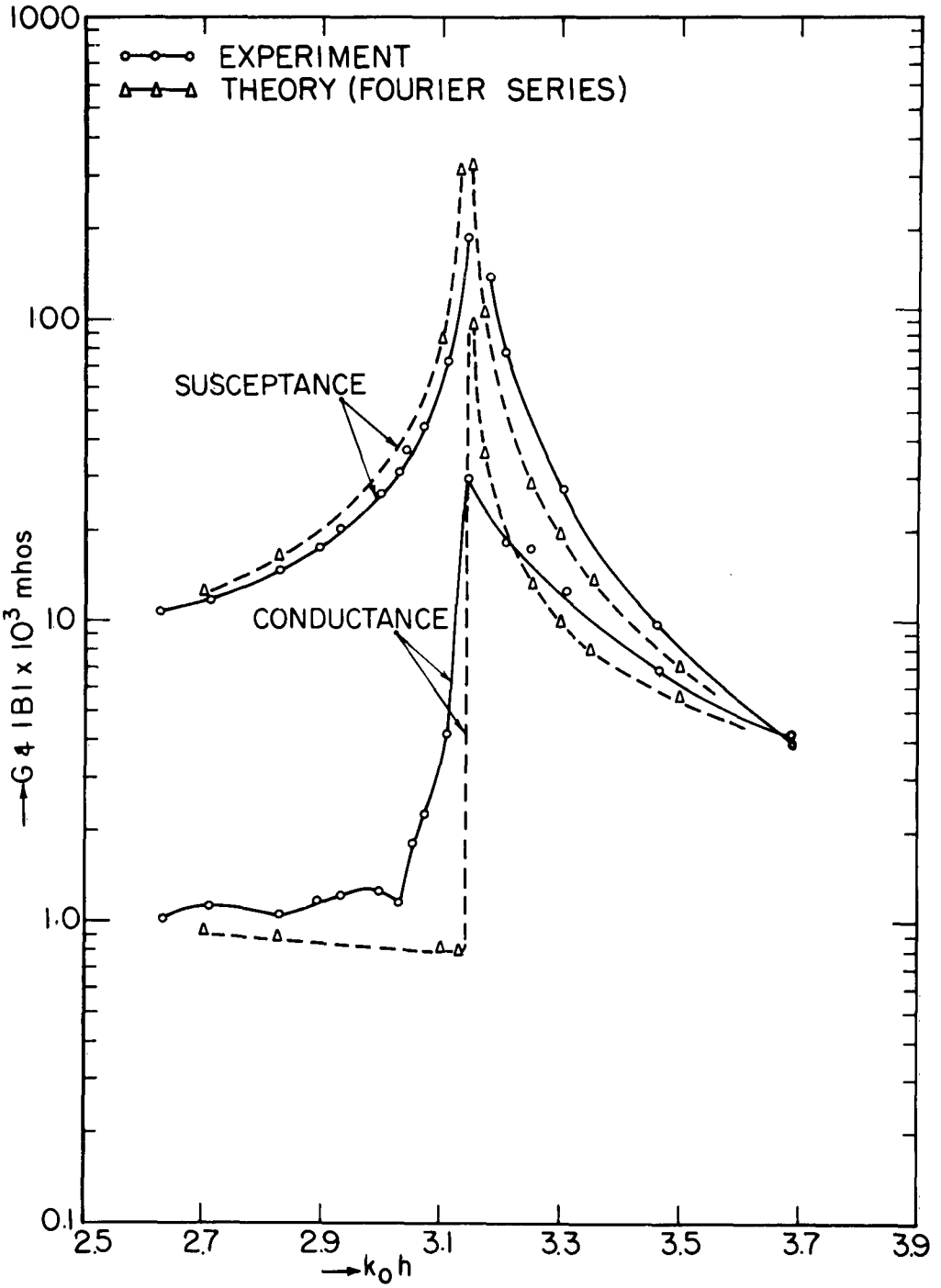

FIG. 1-13 ADMITTANCE BEHAVIOUR AT RESONANCE

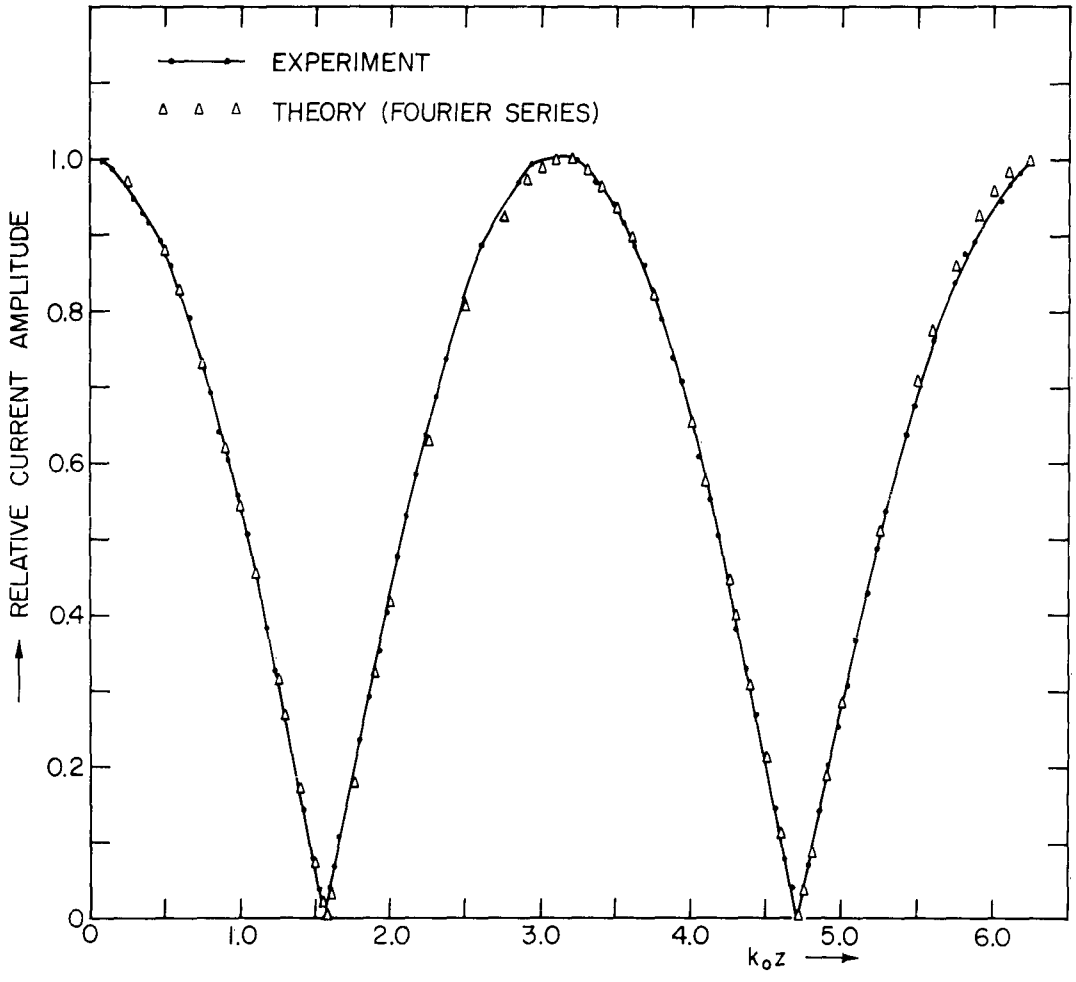

FIG. 1-14 COMPARISON OF THEORETICAL AND EXPERIMENTALLY DETERMINED CURRENT DISTRIBUTION (AMPLITUDE); $k_0h = 2\pi$; $a/\lambda = 0.0105$.

Effect of the Logarithmic Singularity in the Antenna Current

The current as given in Eq. 1.41 can be separated into two parts $I(z) = I_A(z) + I_\infty(z)$. $I_A(z)$ represents the current determined by the impedance of the antenna itself and is given by

$$I_A = \frac{jV}{60k_o h}\left[\frac{1}{j\frac{\pi}{2}J_o(k_o a).H_o^{(2)}(k_o a)} + 2\sum_{m=1}^{M}\left(\frac{1}{\gamma_m^2 I_o(k_o a\gamma_m).K_o(k_o a\gamma_m)} - \frac{2(k_o a)(k_o h)}{\pi\, m}\right).\cos\frac{m\pi z}{h}\right]. \quad (1.51)$$

On the other hand,

$$I_\infty(z) = -\frac{jV}{15\pi}(k_o a).\ln\left\{2\sin(\pi z/2h)\right\} \quad (1.52)$$

represents the current determined by the infinite capacitance of the knife edges of the idealized delta-function generator; it has a singularity at the feed point giving rise to an infinite input admittance. It is to be noted that only the phase-quadrature component of the current is infinite; this means that only the input susceptance is infinite while the input conductance remains finite.

The amplitudes of $|I|$, $|I_A|$ and $|I_\infty|$ for an antenna with $k_o h = \pi/2$ and $a/\lambda = 0.01058$ have been plotted in Fig. 1.16.

Such a singularity in the feed-point current has been investigated by several authors (7, 8, 9, 10). The results obtained here are somewhat at variance with the corresponding case for free-space antenna. The following observations may be made.

1. According to King and Wu[(7) and Duncan (8) the logarithmic term in the case of a free-space antenna is

$$I_{\infty A}(z) = -\frac{jV}{30\pi} (k_o a) \cdot \ln k_o z \qquad (1.53)$$

For the parallel-plate antenna

$$I_{\infty P}(z) = -\frac{jV}{15\pi} (k_o a) \ln \left\{2 \sin (\pi z/2h)\right\}. \qquad (1.52a)$$

The factor 2 missing in 1.52 arises from the fact that a monopole is treated instead of a dipole as in (7). In the parallel-plate case the logarithmic term depends on the height of the antenna (spacing between plates) whereas in the free-space case it is independent of the length of the antenna. This difference is probably due to the imaging effect of the two plates which gives an infinite series of generators separated by a distance h.

2. Though such a singularity in the feed-point current has been predicted theoretically for the free-space antenna, no such phenomenon has been detected by either the Fourier or iterative solutions of the integral equation for the antenna current. Duncan and Hinchey (10) have carried out the Fourier expansion to as high as the 25th order without noticing any untoward behavior.

3. Many of the previous workers have defined a 'transition region' or 'boundary layer region' where the logarithmic function makes a significant contribution. According to Wu and King (7) the transition zone is given by

$$z_s = \lambda/2e^{-1/Ka}. \qquad (1.54)$$

For the antenna used in the experiments $k_o a = 0.0664$ ($a/\lambda = 0.01058$); this gives $k_o z_s = 2.9 \times 10^{-7}$.

According to Duncan (8) the corresponding transition zone for an antenna with $k_o a = 0.01$ is $k_o z_s = 0.008$ ($z_s/\lambda = 0.0013$). He has also shown that $z_s < \lambda/25$ for $h/a \gtrsim 60$. In Fig. 1.15, the amplitude of the current near the driving point measured experimentally for an antenna with $k_o h = \pi/2$ and $a/\lambda = 0.01058$ has been compared with the theoretical results obtained by the Fourier-series method. If the transition zone is defined as the point at which the logarithmic term exceeds the nominal value of the observed current, then from Fig. 1.15 the transition region is $k_o z_s = 0.175$, which is much higher than the values predicted for the free-space antenna.

4. It has been further proposed that in order to get a finite value for the input admittance the logarithmic term in the current distribution should be subtracted out. Such a subtraction process, while valid for thin structures, may be questionable for thick antennas like the one used in the present experiment. In Fig. 1.16, the amplitude of the currents $|I|$, $|I_A|$ and $|I_\infty|$ for an antenna with $k_o h = \pi/2$ and $a/\lambda = 0.01058$ has been plotted. It can be seen that the logarithmic term makes a marked contribution over a significant length of the antenna. In fact, the dip in the current distribution at $k_o z = 0.2$ seems to be due principally to the logarithmic term. However, as the antenna gets thinner the logarithmic

term plays a less significant role because of the factor $k_o a$ in the coefficient; in fact, for an infinitesimally thin antenna it has been shown (see ensuing discussion) that the current distribution becomes a flattened cosine curve.

Admittance of the Antenna

To compare the theoretical values of the admittance with the experimental results we have to subtract out the infinite gap capacitance due to the idealized delta-function generator. Thus, from equation 1.41 we get

$$Y_o = G_o + jB_o = \frac{j}{60k_o h}\left[\frac{1}{j\frac{\pi}{2} \cdot J_o(k_o a).H_o^{(2)}(k_o a)}\right.$$

$$\left. + 2\sum_{m=1}^{M}\left(\frac{1}{\gamma_m^2 I_o(k_o a\gamma_m) \cdot K_o(k_o a\gamma_m)} - \frac{2(k_o a).(k_o h)}{\pi} \cdot \frac{1}{m}\right)\right] . \quad (1.54)$$

However, it is necessary to add to this result a correction term to account for the input susceptance of the actual gap or feed (9, 10). The correction term denoted here by jB_{GAP} may be obtained empirically by comparing the experimental results with the theoretical values for B_o given in equation 1.54. The final theoretical results to be compared with experiment are then

$$Y_F = G_o + j(B_o + B_{GAP}) = G_F + jB_F \quad (1.55)$$

Note $G_o = G_F$.

In Tables 1-2 (A) and 1-2 (B) the gap correction $B_{GAP} = B_{EXP} - B_o \quad (1.56)$

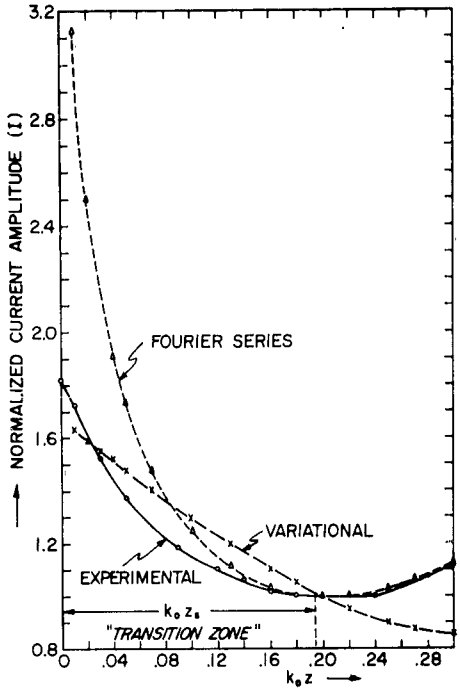

FIG. 1-15 COMPARISON OF THEORETICAL AND EXPERIMENTALLY DETERMINED CURRENT DISTRIBUTION NEAR DRIVING POINT.
$k_o h = \pi/2$; $a/\lambda = 0.01058$; M = 10

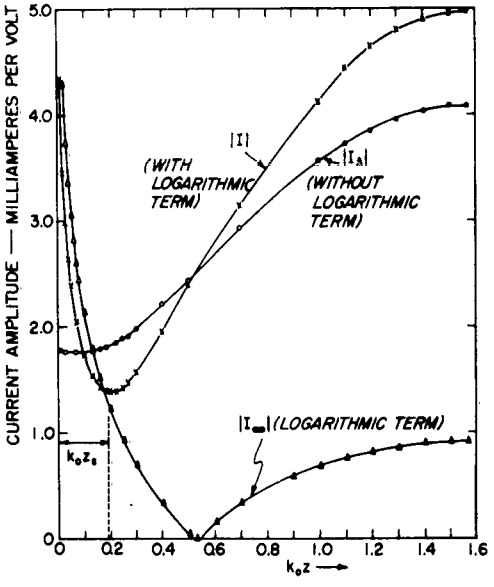

FIG. 1-16 THEORETICAL CURRENT DISTRIBUTION CURVE WITH AND WITHOUT LOGARITHMIC TERM.
$k_o h = \pi/2$; $a/\lambda = 0.0105$; M = 10.

SR15

$B_{GAP} = B_{EXP} - B_o$

B_{EXP} = Experimentally Measured Admittance

B_o = Susceptance After Subtracting Infinite Gap Susceptance Obtained by Fourier-Series Method.

B_{GAP} = Gap Correction Susceptance

A)

$k_o h$	B_o[mhos x 10^3]	B_{EXP}[mhos x 10^3]	B_{GAP}[mhos x 10^3]
0.7854	-j5.49	-j1.10	+j4.29
1.0000	-j3.83	+j0.20	+j4.03
1.2960	-j2.25	+j1.60	+j3.85
1.5708	-j0.99	+j3.10	+j4.09
1.8450	+j0.21	+j4.50	+j4.38
2.0000	+j1.06	+j5.30	+j4.23
2.3562	+j3.34	+j7.60	+j4.25

Average value of B_{GAP} = +j4.10 for $0 < k_o h < \pi$.

B)

$k_o h$	B_o[mhos x 10^3]	B_{EXP}mmhos x 10^3]	B_{GAP}[mhos x 10^3]
3.5000	-j12.41	-j7.40	+j5.01
3.9270	-j6.23	-j0.40	+j5.83
4.3000	-j3.98	+j1.10	+j5.08
4.6200	-j2.55	+j2.80	+j5.35
4.7124	-j2.17	+j3.20	+j5.37
4.9000	-j1.37	+j4.15	+j5.52
5.1000	+j0.47	+j5.40	+j4.92
5.4978	+j2.00	+j5.55	+j5.55

Average value of B_{GAP} = +j5.41 $\pi < k_o h < 2\pi$.

TABLE 1-2 (A) and (B). Evaluation of Gap Correction Susceptance.

has been tabulated. B_{EXP} is the value of susceptance obtained experimentally and B_o is given by Eq. 1.54.

Because of their high values and steep variation, the values of B near resonance have not been taken into account while calculating B_{GAP} lest they should lead to erroneous results.

It can be seen that in the range $0 < k_o h < \pi$, B_{GAP} is nearly constant and has an average value of 4.10×10^{-3} mhos. In the range $\pi < k_o h < 2\pi$, B_{GAP} is again nearly constant but average value is 5.41×10^{-3} mhos. This increase in B_{GAP} correction term is probably due to the fact that when the plate separation is greater than a half-wavelength, there are two modes propagating in the guide which might change the field distribution at the aperture of the driving coaxial line.

Comparison with Experimental Results

In Figure 1-17 the theoretical values of the conductance obtained by the Fourier-series method have been compared with experimental results.

- - - - - - -

TABLE 1-3

$Y_F = G_F + jB_F$ = Fourier-Series Admittance of Antenna

$B_F = B_o + B_{GAP}$

where B_o = Susceptance after Subtracting out Infinite Gap Susceptance Obtained by Fourier-Series Method. B_{GAP} = Empirical Gap Correction Susceptance.

$$B_{GAP} = +j4.102 \qquad \text{for } 0 < k_o h < \pi$$

$$B_{GAP} = +j5.413 \qquad \text{for } \pi < k_o h < 2\pi$$

In Fig. 1.18 and Fig. 1.19, the theoretical values for susceptance B_F (obtained after subtracting infinite gap susceptance and adding the empirical gap correction term) have been compared with measured values. They are found to agree well. The theoretical admittance values obtained by the Fourier-series method have been tabulated in Table 1-3.

Gap Capacitance of the Delta-Function Generator

The logarithmic term in the current distribution due to the delta-function generator may also be written from 1.34 and 1.39 as

$$I_\infty(z) = \frac{j2\pi V}{\zeta_o k_o h}\left[\frac{4(k_o a)\,.\,(k_o h)}{\pi}\,.\sum_{m=1}^{\infty}{}'\,\frac{\cos\frac{m\pi z}{h}}{m}\right]. \qquad (1.57)$$

The gap susceptance is given by

$$Y_\infty(z) = \left[\frac{I_\infty}{V}\right]_{z=0} = j\frac{8}{\zeta_o}\,.\,(k_o a)\,.\sum_{m=1}^{\infty}\frac{1}{m} \qquad (1.58)$$

where

$$\sum_{1}^{M}\frac{1}{m} = \gamma + \ln M\,. \qquad (1.59)$$

γ = Euler's constant = 0.5772 .

Thus

$$Y_\infty = J\frac{8}{\zeta_o}\,.\,(k_o a)\,.\,D \qquad (1.60)$$

where D is an infinite positive constant. It is worth while noting that, as in the free-space case (7), Y_∞ is proportional to the frequency and

$k_o h$	G_F[mhos x 10^3]	jB_o [mhos x 10^3]	jB_F[mhos x 10^3]
0.5000	5.00	-j8.83	-j4.73
0.7854	3.18	-j5.39	-j1.29
1.0000	2.50	-j3.83	+j0.26
1.2960	1.93	-j2.25	+j1.85
1.5708	1.59	-j0.99	+j3.10
1.8450	1.35	+j0.21	+j4.31
2.0000	1.25	+j1.06	+j5.16
2.3562	1.06	+j3.34	+j7.45
2.7000	0.92	+j8.27	+j12.37
2.8250	0.88	+j12.01	+j16.11
3.1000	0.80	+j82.72	+j86.82
3.1300	0.79	+j309.47	+j313.57
3.1500	96.89	-j334.23	-j328.81
3.1700	36.29	-j110.84	-j105.43
3.2500	13.02	-j34.10	-j28.69
3.3000	9.88	-j24.64	-j19.23
3.3570	7.94	-j19.01	-j13.59
3.5000	5.60	-j12.41	-j7.00
3.9270	3.36	-j6.23	-j0.81
4.3000	2.62	-j3.98	+j1.42
4.6200	2.25	-j2.55	+j2.85
4.7124	2.16	-j2.17	+j3.24
4.9000	2.02	-j1.37	+j4.04
5.1000	1.88	+j0.47	+j5.88
5.4978	1.67	+j2.00	+j7.41
5.8000	1.54	+j7.68	+j13.09
6.1500	1.42	-j23.46	-j18.05

TABLE 1-3 Theoretical Admittances of Antenna Determined by Fourier-Series Method; $a/\lambda = 0.01058$; Truncation term $M = 10$.

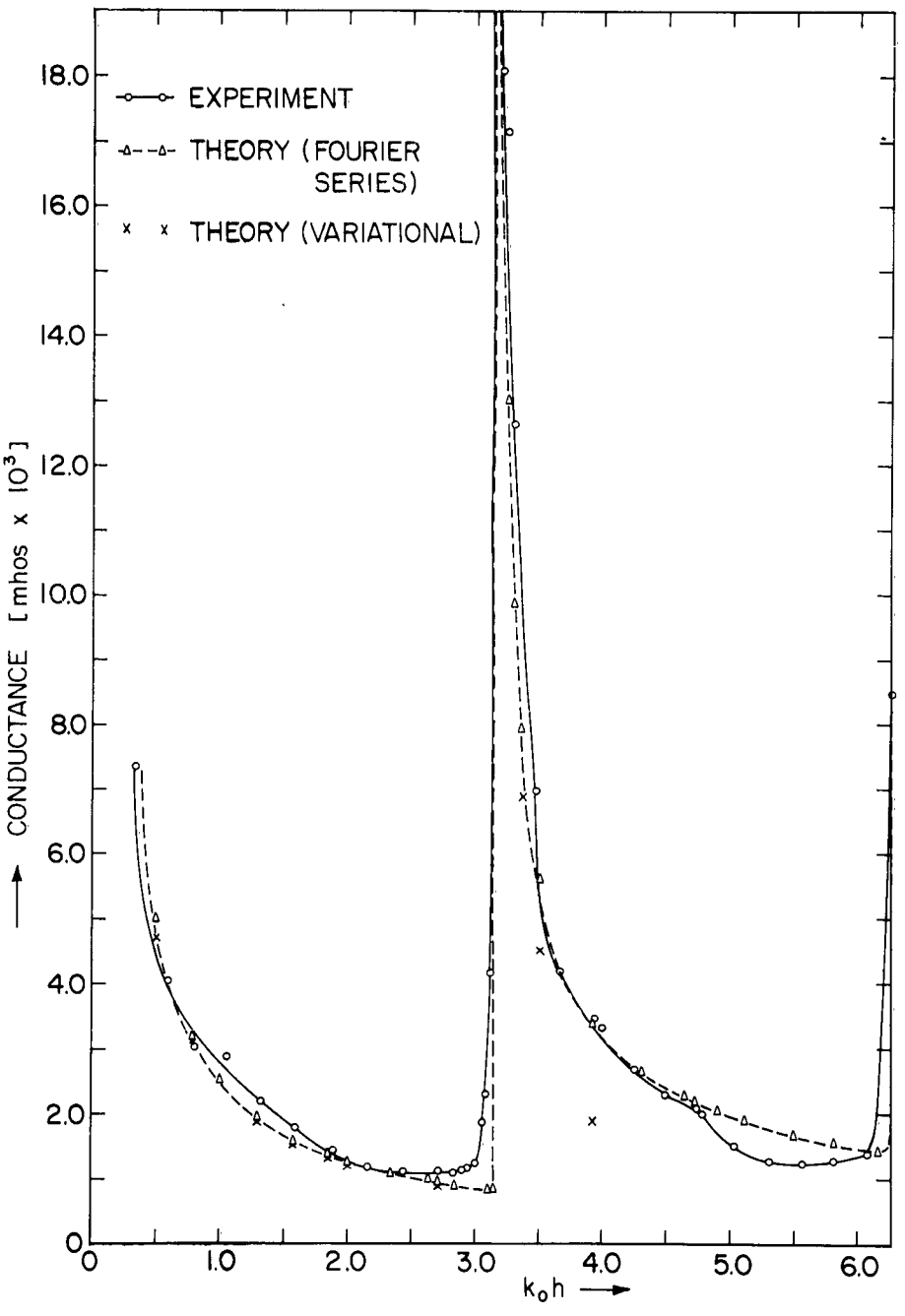

FIG. 1-17 COMPARISON OF THEORETICAL AND EXPERIMENTALLY MEASURED CONDUCTANCE. $a/\lambda = 0.0105$; $M = 10$

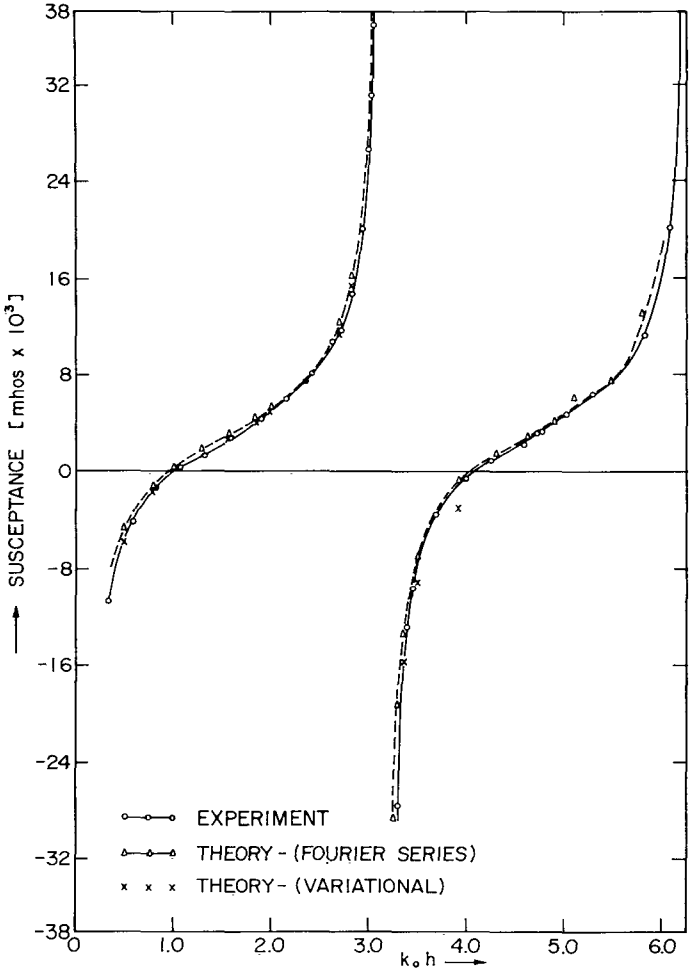

FIG. 1-18 COMPARISON OF THEORETICAL AND EXPERIMENTALLY DETERMINED SUSCEPTANCE. (LINEAR SCALE).

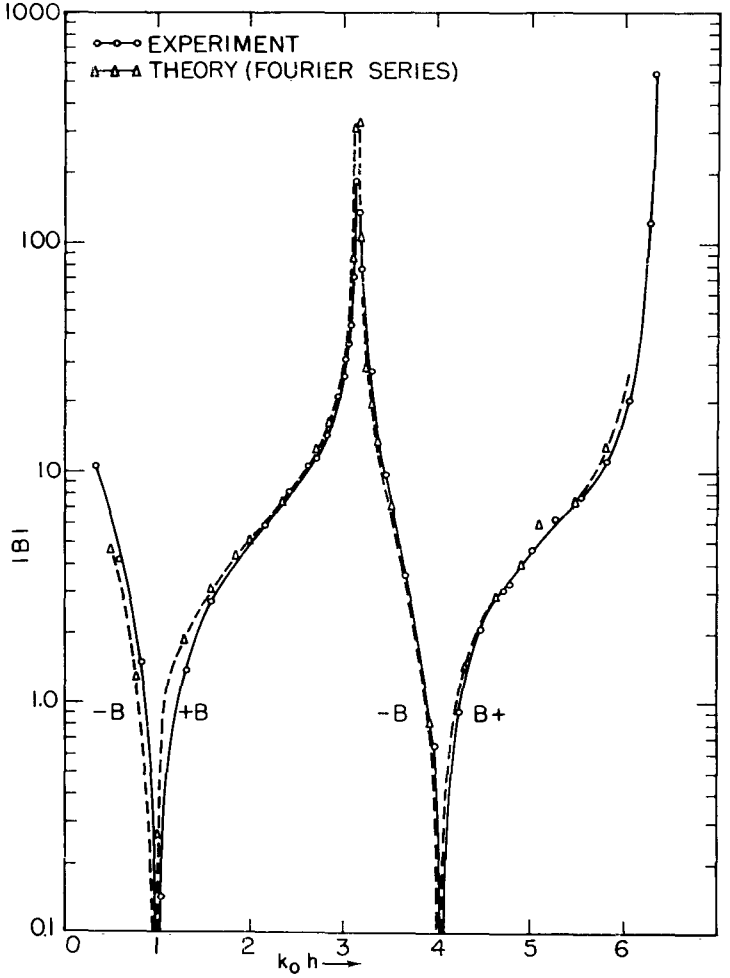

FIG. 1-19 COMPARISON OF THEORETICAL AND EXPERIMENTALLY DETERMINED SUSCEPTANCE. (LOG SCALE)

circumference of the antenna but is independent of the antenna length h.

Since $\zeta_o = \sqrt{\mu_o/\varepsilon_o}$ and $k_o = \omega\sqrt{\mu_o\varepsilon_o}$

the gap capacitance

$$C_\infty = \frac{Y_\infty}{j\omega} = 8\,\varepsilon_o\,a\,D = 8\,\varepsilon_o\,a \lim_{M\to\infty} [\gamma + \ln M]. \qquad (1.62)$$

It has already been noted that a finite gap correction term B_{GAP} must be added to the theoretical susceptance values in order to bring them into agreement with experimental results. For $0 < k_o h < \pi$ the correction term evaluated empirically from experimental results is 4.10×10^{-3} mhos.

$$B_{GAP} \simeq \frac{j}{15\pi} \cdot (k_o a) \cdot [\gamma + \ln m] \simeq 4.10 \times 10^{-3} \text{ mhos.}$$

The corresponding value of $m = 10.74 \simeq 10$.

Thus, the gap correction to be added to Y_o in Eq. 1.54 is

$$B_{GAP} = j/60\, k_o h \cdot \frac{4(k_o a)\,(k_o h)}{\pi} \sum_{m=1}^{10} \frac{1}{m} = 4.1 \times 10^{-3} \text{ mhos.}$$

This is exactly the last term on the right-hand side of Eq. 1.54 which was subtracted out. This means that in Eq. 1.35 we need add only the first 10 terms, which represents the contribution to the susceptance from the first 10 higher-order modes, to get results for the susceptance which agree with the experimentally measured values.

Current Distribution on an Infinitesimally Thin Antenna

The general expression for the current distribution on the antenna is given by (1.34). Consider now the term in this equation which involves the series summation and denote it by S .

$$S = 2 \sum_{m=1}^{\infty}{}' \frac{\cos m\pi z/h}{\gamma_m^2 \cdot I_o(k_o a\gamma_m) \cdot K_o(k_o a\gamma_m)} \quad . \tag{1.63}$$

For small arguments, $K_o(x) = \log(\beta x)$, and $I_o(x) \sim 1$, where $\log \beta = \gamma - \log 2 \simeq -0.1159$.

$$\gamma_m \sqrt{\left(\frac{m\pi}{k_o h}\right)^2 - 1} \sim \frac{m\pi}{k_o h} .$$

Hence ,

$$\beta k_o a\gamma_m = \left(\frac{\beta a \pi}{h}\right) \cdot m$$

and

$$\log(\beta k_o a\gamma_m) = \log\left(\frac{\beta a \pi}{h}\right) + \log m \quad . \tag{1.64}$$

We note that as $a \to 0$, $\log(\beta a\pi/h) \to \infty$.

This means that for an infinitesimally thin antenna, with vanishing radius, the $\log(\beta a\pi/h)$ term completely predominates over the $\log m$ term.

Therefore,

$$\log(\beta k_o a\gamma_m) \sim \log(\beta a\pi/h) \quad . \tag{1.65}$$

Thus, for thin antennas

$$S = 2 \sum_{m=1}^{\infty} \frac{-\cos m\pi z/h}{\left[(m\pi/k_o h)^2 - 1\right]\left[\log(\beta k_o a \gamma_m)\right]}$$

$$= \frac{-2\left(\frac{k_o h}{\pi}\right)}{\log\left(\frac{\beta a \pi}{h}\right)} \cdot \sum_{m=1}^{\infty} \frac{\cos m\pi z/h}{\left[m^2 - \left(\frac{k_o h}{\pi}\right)^2\right]} \quad . \tag{1.66}$$

If the following summation formula, viz.,

$$\sum_{n=1}^{\infty} \frac{\cos nx}{n^2 - a^2} = \frac{1}{2a^2} - \frac{\pi}{2a} \frac{\cos(x - \pi)a}{\sin \pi a} \tag{1.67}$$

$$0 \leq x \leq 2\pi$$

is used, the result is

$$S = -1/\log(\beta a\pi/h) + \frac{k_o h}{\log\left(\frac{\beta a\pi}{h}\right)} \cdot \frac{\cos k_o(h-z)}{\sin k_o h} \quad . \tag{1.68}$$

For small arguments, $J_o(x) \sim 1$ and $H_o^{(2)}(x) \sim 1 - j\frac{2}{\pi} \log(\beta x)$. With 1.34 , 1.68 , and these identities the current distribution on an infinitesimally thin antenna in a parallel-plate region is given by

$$I(z) = \frac{jV}{60 k_o h} \left\{ \frac{1}{j\frac{\pi}{2} + \log(\beta k_o a)} - \frac{1}{\log\frac{\beta a\pi}{h}} + \left[\frac{k_o h}{\log\frac{\beta a\pi}{h} \cdot \sin k_o h}\right] \cos k_o(h - z) \right\} . \tag{1.69}$$

This is of the form $I(z) = A + B \cos k_o (h - z)$, and the current distribution is a slightly flattened cosine curve.

Current Distribution with a Filamentary Kernel

In the solution of the integral equation for the antenna current using iterative methods, it is customary to replace the correct kernel distance of the form 1.10 by an approximate 'filamentary' kernel distance (1, 8) given by

$$R_m = \sqrt{(z \pm z' - 2mh)^2 + a^2} \quad . \tag{1.70}$$

It is assumed that $h >> a$.

While such an approximation may be valid for the free-space antenna problems, it leads to divergence difficulties in the current in the case of wave-guide probe investigations. Thus, if 1.70 is substituted in 1.5 and the manipulations carried out the current distribution on the antenna comes out as

$$I(z) = \frac{jV}{60k_o h} \left\{ \frac{1}{j\frac{\pi}{2} H_o^{(2)}(k_o a)} + 2 \sum_{m=1}^{\infty} \frac{\cos m\pi z/h}{\gamma_m^2 . K_o(k_o a \gamma_m)} \right\} . \tag{1.71}$$

For higher values of m, $\gamma_m \simeq m\pi / k_o h$ and

$$k_o a \gamma_m \simeq \frac{\pi a}{h} \cdot m \ .$$

The asymptotic expansion for $K_o(x)$ is

$$(\pi / 2x)^{1/2} \ e^{-x} \ ;$$

therefore, $1/K_o(k_o a \gamma_m) \ . \ \gamma_m^2$ behaves like

$$2\sqrt{(k_o a)\,.\,(k_o h)^3}\,.\left[\frac{e^{+(\pi a/h).m}}{m^{3/2}}\right].$$

Thus, the series for the current distribution diverges. Such a divergence difficulty has been noticed by Lewin (4) while investigating the problem of a probe in a waveguide.

Distribution of Charge on the Antenna

The charge distribution may be obtained directly from the equation of continuity

$$\frac{dI_z}{dz} + j\omega q_z = 0 \qquad (1.72)$$

where $I_z = I''_z + jI'_z$ is given by Eq. 1.34. Thus from 1.72 the distribution of charge

$$q(z) = j(q''_z + jq'_z) = \frac{j}{\omega}\left(\frac{\partial I''_z}{\partial_z} + j\frac{\partial I'_z}{\partial_z}\right)$$

so that for $0 < k_o h < \pi$

$$q''_z = \frac{1}{\omega}\,\frac{\partial I''_z}{\partial z} = 0. \text{ Since } I''(z) \text{ is a constant for } k_o h < \pi. \qquad (1.73)$$

$$q'_z = \frac{1}{\omega}\,\frac{\partial I'_z}{\partial z} = -\frac{V}{30\omega}\cdot\frac{\pi}{(k_o h)^2}\left[\sum_{m=1}^{\infty}\frac{m\sin m\pi z/h}{\gamma_m^2 I_o(k_o a\gamma_m)K_o(k_o a\gamma_m)}\right]$$

The charge distribution, being sinusoidal, is maximum near the center and vanishes at the ends. When $k_o h > \pi$, $q''_z \neq 0$ because of the contribution from the first higher-order mode $m \simeq 1$.

3. VARIATIONAL METHOD

It has been shown in Section 2 that while the Fourier-series method gives accurate solutions for the current distribution and conductance of the antenna, the values for the susceptance obtained from it are ambiguous because of the feed-point singularity in the current. The variational technique, however, like the one employed by J. Storer (11) in the case of a free-space antenna, ignores the singularity of the driving point and provides an approximate but continuous solution for the current distribution over the entire length of the antenna.

The stationary expression for impedance can be formulated in the following manner:

$$V_o \, \delta(z) = j\zeta_o \int_o^h K(z, z') \, I(z') \, dz' .$$

The driving voltage $V_o = Z_o I_o$ where Z_o is the input impedance and I_o - input current. Therefore,

$$Z_o I_o \, \delta(z) = j\zeta_o \int_o^h K(z, z') \, I(z') \, dz' \quad . \tag{1.75}$$

If both sides are multiplied by I(z) and integrated between 0 and h and then divided through by $I^2(0)$ the result is

$$Z_o = \frac{1}{I_o^2} \, j\zeta_o \int_o^h \int_o^h K(z, z') \, I(z) \, I(z') \, dz \, dz' \tag{1.76}$$

where $K(z, z')$ is the kernel given by 1.29 and 1.30. Since the kernel is symmetric, i.e., $K(z, z') = K(z', z)$, Eq. 1.76 can be shown to have all the variational characteristics, and Z_o is stationary with respect to small changes in I_z.

According to 1.34 and 1.69, a suitable trial function for the current is

$$I_T(z) = A + B \cos k_o (h - z) \quad . \tag{1.77}$$

With this type of current distribution the impedance is given by

$$\bar{Z}_V = \frac{1}{I_T^2(0)} \; j\zeta_o \left[\int_o^h \int_o^h K(z, z') \left[A + B \cos k_o(h-z) \right] \left[A + B \cos k_o(h-z') \right] dz\, dz' \right.$$

$$\bar{Z}_V = \frac{j\zeta_o}{I_T^2(0)} \left[A^2 \nu_{AA} + 2A.B\nu_{AB} + B^2 \nu_{BB} \right] \tag{1.78}$$

where

$$\nu_{AA} = \int_o^h \int_o^h K(z, z')\, dz\, dz' \tag{1.79}$$

$$\nu_{AB} = \int_o^h \int_o^h K(z, z') \,.\, \cos k(h-z) \,.\, dz\, dz'$$

$$= \frac{1}{2} \int_o^h \int_o^h K(z, z') \left[\cos k_o(h-z) + \cos k(h-z') \right] dz\, dz' \tag{1.80}$$

$$\nu_{BB} = \int_0^h \int_0^h K(z, z') \cos k_o(h - z). \cos k_o(h - z') \, dz \, dz' . \quad (1.81)$$

The two complex coefficients for the trial current A and B have to be determined in order to calculate the impedance from (1.78). It is assumed that a unit voltage is driving the antenna; the current at z = 0 is determined by the following condition:

$$V = 1 = I_T(0) . \bar{Z}_V .$$

$$I_T(0) = A + B \cos k_o h = 1/\bar{Z}_V . \quad (1.82)$$

From (1.82)

$$A = \left[\frac{1}{\bar{Z}_V} - B \cos k_o h \right] . \quad (1.83)$$

$$Z_V = j\zeta_o \frac{1}{(\bar{Z})^2} \left\{ \nu_{AA} \left[\frac{1}{\bar{Z}_V} - B \cos k_o h \right]^2 + 2\nu_{AB} . B \left[\frac{1}{\bar{Z}_V} - B \cos k_o h \right] + \nu_{BB} . B^2 \right\} . \quad (1.84)$$

$\bar{Z}_V$ is an analytical function of the parameter B. Thus, the next step is to equate $\frac{\partial \bar{Z}}{\partial B}$ to zero and solve for the optimum value of B which makes $\bar{Z}_V$ stationary.

We obtain

$$B = \frac{1}{\bar{Z}_V} \frac{\left[\nu_{AA} \cos k_o h - \nu_{AB} \right]}{\Delta} . \quad (1.85)$$

where $\Delta = \nu_{AA} \cos^2 k_o h - 2\nu_{AB} \cos k_o h + \nu_{BB}$. (1.86)

Using (1.85) and (1.83) we get

$$A = \frac{1}{\bar{Z}_V} \quad \frac{\left[\nu_{BB} - \nu_{AB} \cos k_o h\right]}{\Delta} \quad . \tag{1.87}$$

If (1.87) and (1.85) are substituted in (1.78) the result is

$$\bar{Z}_V = j\zeta_o \quad \frac{\left[\nu_{AA} \cdot \nu_{BB} - \nu_{AB}^2\right]}{\Delta} \quad . \tag{1.88}$$

Evaluation of the 'ν' integrals

The various ν integrals occurring in the above equations can now be evaluated; the following simple integrals will prove useful in the derivation:

$$\int_o^h \cos k_o(h - z)\, dz = \sin k_o h / k$$

and

$$\int_o^h \sin k_o (h - z) \cos \frac{m\pi z}{h} \, dz = \frac{\sin k_o h}{k_o\left[1 - (m\pi / k_o h)^2\right]} . \tag{1.89}$$

From Eq. 1.79 we have

$$\nu_{AA} = \int_o^h \int_o^h K(z, z')\, dz\, dz' = \frac{-jk_o h}{4} \; J_o(k_o a)\, H_o^{(2)}(k_o a) . \tag{1.90}$$

From (1.80)

$$\nu_{AB} = \int_0^h \int_0^h K(z, z') \cos k_o(h - z)\, dz\, dz'$$

$$= - j \frac{\sin k_o h}{4} \; J_o(k_o a) \cdot H_o^{(2)}(k_o a) \qquad (1.91)$$

$$0 < k_o h < 2\pi .$$

From (1.81)

$$\nu_{BB} = \int_0^h \int_0^h K(z, z') \cos k_o(h-z) \cos k_o(h-z')\, dz\, dz'$$

$$= \frac{-1}{2\pi k_o h} \left\{ j \frac{\pi}{2} J_o(k_o a) \cdot H_o^{(2)}(k_o a) \cdot \left(\frac{\sin k_o h}{k_o} \right)^2 \cdot \right.$$

$$\left. + 2 \sum_{m=1}^{\infty} \frac{I_o(k_o a \gamma_m) \cdot K_o(k_o a \gamma_m)}{\gamma_m^2} \sin^2 k_o h \right\} \quad \text{for } 0 < k_o h < \pi .$$

For higher-order terms

$$I_o(k_o a \gamma_m) \cdot K_o(k_o a \gamma_m) \simeq \frac{1}{2 k_o a \gamma_m} \simeq \frac{k_o h}{2(k_o a) \cdot m\pi}$$

Therefore

$$\sum_{m=M}^{\infty} \frac{I_o(k_o a \gamma_m) \cdot K_o(k_o a \gamma_m)}{\gamma_m^2} = \frac{(k_o h)^3}{2(k_o a) \cdot \pi^3} \left[\sum_{m=1}^{\infty} \frac{1}{m^3} - \sum_{m=1}^{M} \frac{1}{m^3} \right]$$

where M is the truncation term in the series.

Now $\sum_{m=1}^{\infty} \frac{1}{m^3} = \zeta(3) = 1.202$

where $\zeta(s)$ is the Riemann Zeta function (12) defined by

$$\zeta(s) = 1 + 1/2^s + \frac{1}{3^s} + \cdots \quad \text{when } s > 1.$$

Therefore for $0 < k_o h < \pi$

$$\nu_{BB} = \frac{-\sin^2 k_o h}{2\pi k_o h} \left\{ j \frac{\pi}{2} J_o(k_o a) . H_o^{(2)}(k_o a) + 2 \sum_{m=1}^{M} \left[\frac{I_o(k_o a \gamma_m) . K_o(k_o a \gamma_m)}{\gamma_m^2} - \frac{(k_o h)^3}{2\pi^3 . k_o a} \cdot \frac{1}{m^3} \right] + 1.202 \frac{(k_o h)^3}{\pi^3 . k_o a} \right\} . \quad (1.92)$$

For $\pi < k_o h < 2\pi$

$$\nu_{BB} = \frac{-\sin^2 k_o h}{2\pi k_o h} \left\{ j \frac{\pi}{2} J_o(k_o a) . H_o^{(2)}(k_o a) + 2 \left[\frac{j\pi/2 . J_o\left(k_o a \sqrt{1 - (\pi/k_o h)^2}\right) . H_o^{(2)}\left(k_o a \sqrt{1 - (\pi/k_o h)^2}\right)}{\left\{1 - (\pi/k_o h)^2\right\}} - \frac{(k_o h)^3}{2 . (k_o a) . \pi^3} \right] \right.$$

$$+ 2 \sum_{m=2}^{M} \left(\frac{I_o (k_o a \gamma_m) . K_o (k_o a \gamma_m)}{\gamma_m^2} - \frac{(k_o h)^3}{2\pi^3 . k_o a} \cdot \frac{1}{m^3} \right)$$

$$+ 1.202 \quad \frac{(k_o h)^3}{\pi^3 . (k_o a)} \Bigg\} \qquad (1.93)$$

The numerical evaluation of the admittance $Y_V = 1/Z_V = G_V + jB_V$ and the current distribution parameters A and B has been carried out for $k_o a = 0.0664$ ($a/\lambda = 0.01058$) with $M = 10$. The numerical values of A and B are given in Table 1-4 and they are plotted in Fig. 1-20. From Figures 1-17, 1-18, and 1-19, it is seen that the theoretical admittance values are in good agreement with experimental results until $k_o h = 3.7$ but deteriorate rapidly thereafter. The theoretical admittance values are tabulated in Table 1-5. Thus, the trial function for the current of the form $A + B \cos k_o (h - z)$ is valid only in the range $0 < k_o h < 3.7$ but a modification will probably have to be made for longer lengths, to account for the first-order mode which propagates when $k_o h > \pi$. In Table 1-6, the theoretical value for the susceptance B_{VAR} obtained by the variational method are compared with the susceptance values B_o obtained by the Fourier-series method. The difference $B_{VAR} - B_o$ is almost constant up to $k_o h = 2.8250$ and the average value of $B_{Vo} = +j3.63$; this compares favorably with the gap correction term $B_{GAP} = +j4.10$ that has to be applied to B_o obtained by the Fourier-series method.

The average difference $|B_\Delta| = |B_{EXP} - B_V|$ is only $|0.35|$ millimhos indicating good agreement. In Table 1-7 susceptance B_{VAR} obtained by the variational method has been compared with experimental results. The current distribution for an antenna with $k_o h = \pi/2$ and $k_o a = 0.066$ has been calculated from 1.77 and the results are compared with the experimental curve in Fig. 1.21. It can be seen that the general agreement is not as good as it was in the case of the Fourier-series solution Fig. 1-6. In Fig. 1-15 the current near the driving point has been compared with the experimental curve and the Fourier-series solution. Though the qualitative agreement with experiment is rather poor, the variational method does not show any abrupt 'logarithmic' rise near the feeding point as in the case of the Fourier-series solution. It is interesting to note that it is possible to obtain the far-field radiation pattern of the antenna in terms of A and B.

Impedance of a Very Short Antenna

When the plate separation is small we may assume the current on the antenna to be a constant. If we also assume a thin antenna, then

$$Z = \frac{jk_o\zeta_o}{I^2(0)} \cdot \frac{I^2(0)}{2\pi h} \cdot \left\{ \int_o^h \int_o^h j\frac{\pi}{2} J_o(k_o a).H_o^{(2)}(k_o a)\, dz\, dz' - 2\sum_{m=1}^{\infty} I_o(k_o a\gamma_m).K_o(k_o a\gamma_m)\,\gamma_m^2 \int_o^h \int_o^h \cos\frac{m\pi z}{h} \cdot \cos\frac{m\pi z'}{h}\, dz\, dz' \right\} \quad (1.94)$$

$$Z = 30\pi\ (k_o h)\ J_o\ (k_o a)\ .\ H_o^{(2)}\ (k_o a) \quad .$$

For $k_o a << 1$, $J_o\ (k_o a) \sim 1$.

$$H_o^{(2)}\ (k_o a) = 1 - j\ .\ \frac{2}{\pi}\ \left\{ - 0.1159 + \log k_o a \right\}$$

Hence, the impedance of the antenna

$$Z = 30\pi\ (k_o h) + j\,60\, k_o h\ .\ \log\ (1/\beta k_o a) \quad . \qquad (1.95)$$

The above result is the familiar formula for the impedance per length h of an infinitely long wire carrying a uniform current.

$k_o h$	$A \times 10^3$		$B \times 10^3$	
0.5000	0.496	+j3.900	-0.368	-j41.221
0.7854	3.366	+j12.293	-0.239	-j20.105
1.0000	17.334	+j10.336	-17.643	-j17.650
1.2960	1.948	+j4.292	-0.031	-j10.446
1.5708	1.650	+j2.776	-0.011	-j8.873
1.8450	1.361	+j1.826	+0.012	-j8.195
2.0000	1.254	+j1.457	-0.003	-j8.161
2.3562	1.064	+j0.813	-0.004	-j9.085
2.7000	0.907	+j0.315	+0.528	-j11.919
2.8250	0.753	+j0.553	+7.094	-j14.850
3.3570	0.315	-j0.344	-6.584	+j15.703
3.5000	0.262	-j0.335	-4.525	+j9.510
3.9270	0.207	-j0.495	-2.392	+j3.625
4.3000	0.316	-j0.814	-1.253	+j1.185
4.6200	0.854	-j0.018	+1.504	-j0.440
4.7124	1.154	-j0.993	+2.931	-j0.173
4.9000	1.374	-j0.360	+4.306	+j2.784
5.1000	1.234	+j0.080	+4.091	+j5.310
5.4978	0.702	+j0.207	+0.993	+j5.686
5.8000	0.594	+j0.252	+2.335	+j13.200

TABLE - 1-4 . Current Distribution Parameters

A and B in $I_T = A + B \cos k_o (h - z)$.

SR15

$Y_V = G_V + jB_V$ = Variational Admittance

$k_o h$	G_V[mhos x 10^3]	B_V[mhos x 10^3]
0.5000	4.71	-5.89
0.7854	3.18	-1.76
1.2960	1.94	+1.45
1.5708	1.60	+2.77
1.8450	1.35	+4.04
2.0000	1.26	+4.85
2.3562	1.06	+7.23
2.7000	0.92	+11.44
2.8250	0.89	+15.42
3.3570	6.88	-15.69
3.5000	4.52	-9.25
3.9270	1.89	-3.06
4.3000	0.81	-1.27
4.6200	0.72	-1.03
4.7124	1.15	-0.99
4.9000	2.17	+0.16
5.1000	2.78	+2.08
5.4978	2.05	+5.60
5.8000	2.66	+11.94

TABLE 1-5. Theoretical Admittance of Antenna Determined by Variational Method; $a/\lambda = 0.01058$; Truncation Term M=10.

$$B_{Vo} = B_{VAR} - B_o$$

B_{VAR} = Susceptance Obtained by Variational Method

B_o = Susceptance after Subtracting Infinite Gap Capacitance Obtained by Fourier-Series Method.

$k_o h$	$B_{Vo} = B_{VAR} - B_o$
0.7854	+j3.63
1.2960	+j3.70
1.5708	+j3.76
1.8450	+j3.79
2.0000	+j3.79
2.3562	+j3.89
2.7000	+j3.17
2.8250	+j3.31

Average value of B_{Vo} = + j3.63

TABLE 1-6. Comparison of Susceptance B_{VAR} Obtained by the Variational Method with the Susceptance B_o after Subtracting Infinite Gap Susceptance Obtained by Fourier-Series Method.

$$B_{\Delta} = B_{EXP} - B_{VAR}$$

B_{VAR} = Susceptance Obtained by Variational Method

B_{EXP} = Measured Susceptance

$k_o h$	B_{VAR}[mhos x 10^3]	B_{EXP}[mhos x 10^3]	$B_{EXP}-B_{VAR}$ $=B_{\Delta}$[mhos x 10^3]
0.7854	-j1.76	-j1.10	+j0.66
1.2960	+j1.45	+j1.60	+j0.15
1.5708	+j2.77	+j3.10	+j0.33
1.8450	+j4.04	+j4.50	+j0.46
2.0000	+j4.85	+j5.30	+j0.45
2.3562	+j7.23	+j7.60	+j0.37
2.7000	+j11.44	+j11.50	+j0.06
2.8250	+j15.42	+j15.00	-j0.42
3.3570	+j15.69	-j15.50	+j0.19

Average value of $|B_{\Delta}|$ = 0.35 millimhos

TABLE 1-7. Comparison of Susceptance B_{VAR} Obtained by the Variational Method with the Experimentally Measured Susceptance B_{EXP} (a/λ = 0.01058; M = 10).

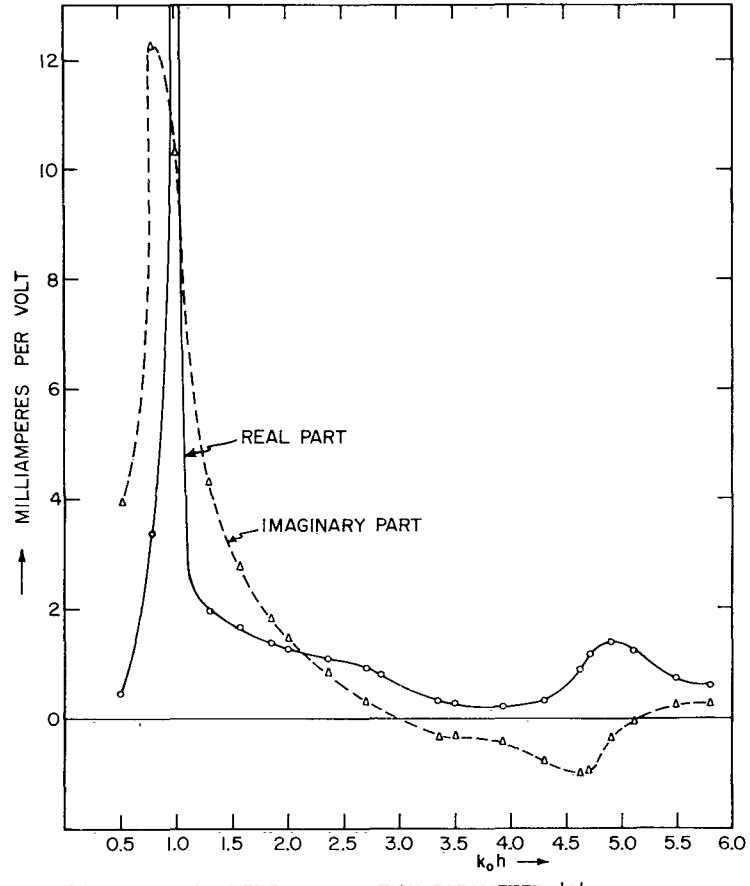

FIG. I-20a CURRENT DISTRIBUTION PARAMETER 'A'.
$a/\lambda = 0.0105$; M = 10.

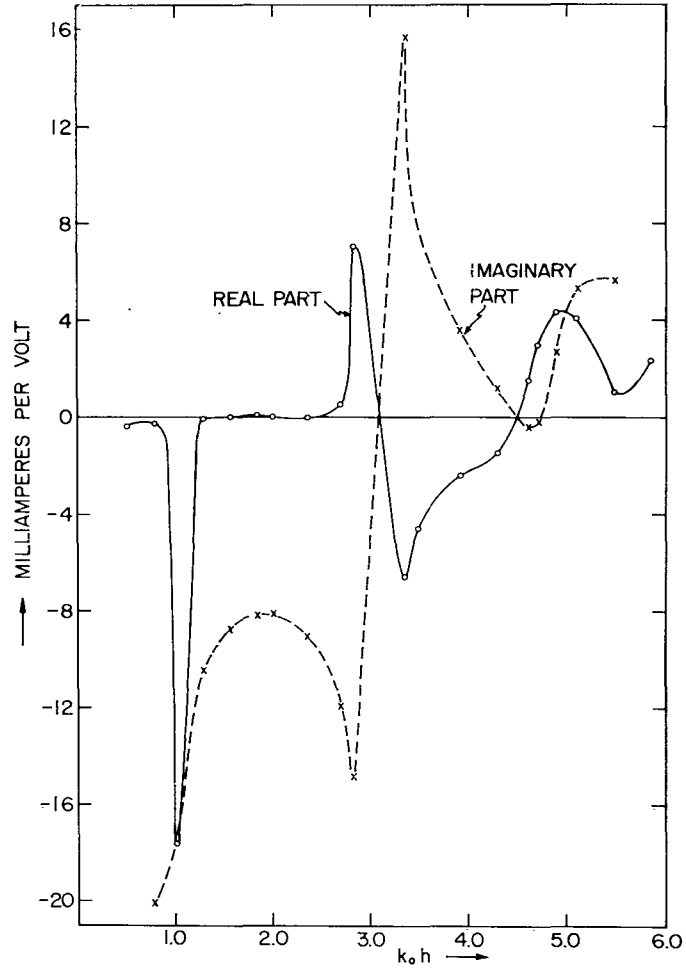

FIG. I-20b CURRENT DISTRIBUTION PARAMETER 'B'.
$a/\lambda = 0.0105$; M = 10.

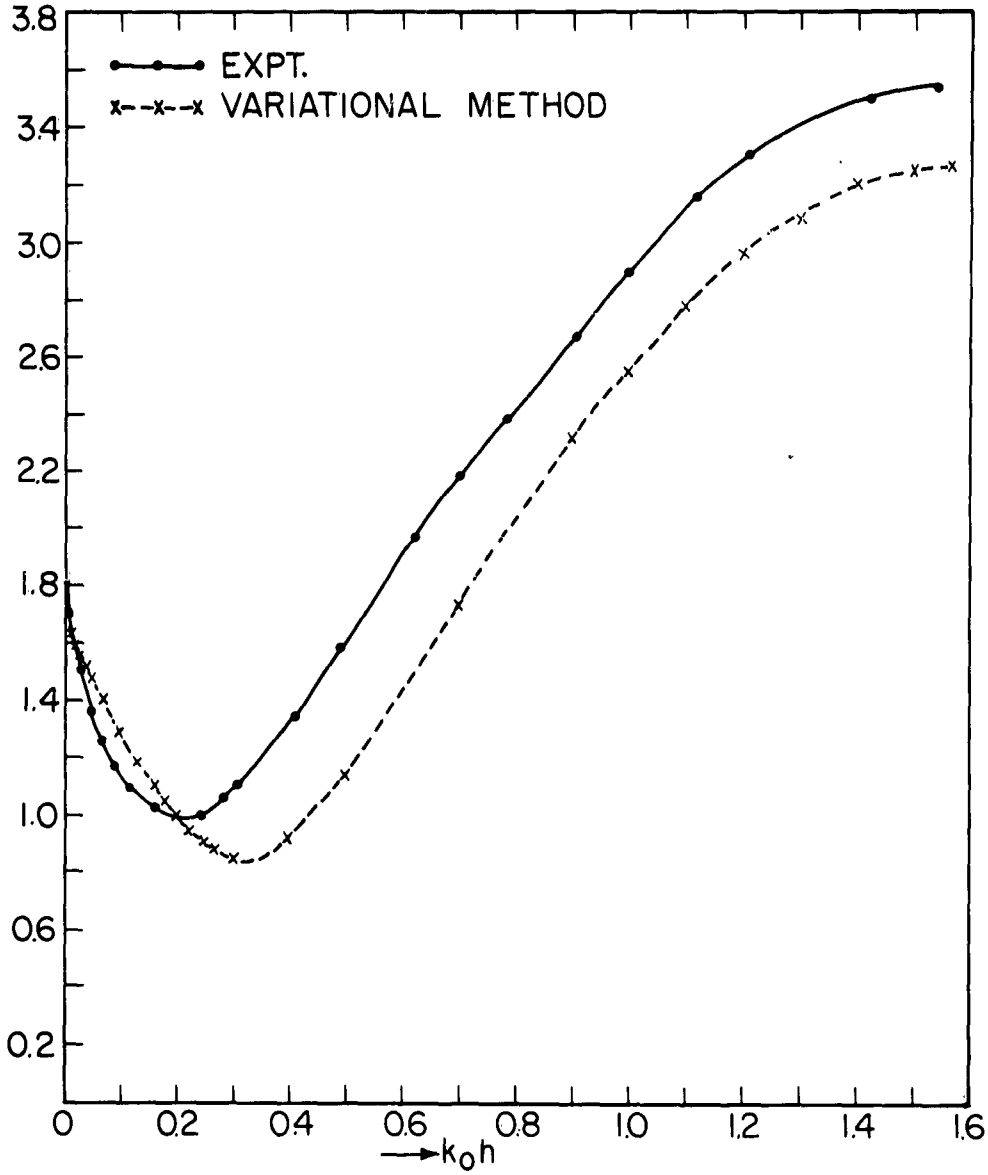

FIG. 1-21 COMPARISON OF THEORETICAL (VARIATIONAL) AND EXPERIMENTAL CURRENT DISTRIBUTION; $k_0h = \pi/2$; $a/\lambda = 0.0105$; $M = 10$

4. EXPERIMENTAL EQUIPMENT AND MEASURING TECHNIQUES

This section is devoted to the experimental phase of this research. The experimental arrangement can be divided into two major groups: 1. The parallel-plate region with the associated absorbing wedges for reducing edge reflections; 2. The coaxial measuring line and ancillary equipment for measuring the input admittance and current distribution of the antenna.

Choice of Frequency

The experimental design of the equipment was complicated by the problem of selecting a suitable frequency which was a compromise between two contradictory factors -

1. It was not practically convenient to have ground planes larger than 6 ft. square because of the size limitations of the laboratory room; hence, the frequency had to be high enough so that the error due to the finite size of the ground planes was not very significant. Besides, inordinately large and heavy ground planes were undesirable since it would then be very difficult to vary the plate separation without resorting to complicated mechanical devices. Moreover, as the frequency decreases it becomes increasingly difficult to find suitable absorbing material to terminate the rims of the parallel-plate region to minimize edge reflections.

2. The frequency at the same time had to be sufficiently low in order not to limit the accuracy of the measuring equipment, because of the mechanical tolerances involved and to minimize deleterious effects like probe loading and large end-corrections. Furthermore, the plate spacing had to be varied by small fractions of a wavelength in order to study the behavior of the input admittance of the antenna as a function of its length; this could be accomplished more easily at longer wavelengths.

It was proposed to carry out the measurements at a frequency of 1000 Mcs. (L Band) which seemed to be a reasonable compromise between these two extremes and had the additional advantage that convenient oscillators were readily available.

Design and Construction of the Parallel-Plate Region

The error due to the plates being finite instead of infinite as theoretically required is difficult to estimate as no adequate experimental data are available. However, from a study of the results obtained for antenna impedance measurements in free space it was decided that the minimum size of the plates should be six wavelengths to obtain reasonably accurate results. Meier and Summers (13) have studied the effect of screens smaller than 6λ on the measured input admittance of antennas in free space. For a square ground plane of side 6λ they have reported a maximum error of 1Ω for a thin antenna of length $h/\lambda = 0.224$ and an error of $\pm$ 25 ohms for a length of $h/\lambda = 0.448$. The percent error in $|Z|$ could thus be

almost 3 % ; the errors are found to be slowly damped oscillatory functions of the dimensions of the ground screen. The corresponding errors in the case of a parallel-plate region are likely to be of a lower order of magnitude since the edge reflections can be virtually eliminated by using absorbing wedges. To reduce the error further the antenna was mounted off-center by a quarter-wavelength. Andrews(14) reports that for an antenna placed off-center the error varies as d^{-2} where d represents the side dimension of the image plane.

In accordance with the above requirements the over-all dimensions of the parallel-plate device were made 6 feet x 6 feet (or approximately 6 wavelengths square at 1000 Mc). Actually the bottom plate measured 6 feet x 12 feet (6λ x 12λ) and was fabricated from $\frac{1"}{4}$ Dural sheets mounted on a sturdy wooden framework to prevent sagging. To enable the measurement of the standing-wave ratio inside the parallel-plate region the lower plate was divided lengthwise by a sliding panel made from $\frac{1"}{4}$ Dural sheet $6\frac{1}{2}$ feet long x 1 inch wide. The panel carried a small electric probe near its center and could be driven by means of a geared-down motor and a cable sliding over a pulley. The position of the probe could be determined to 0.1 mm by means of a steel scale and a vernier mounted on the lower plate. Fig. 1.22 shows a picture of the sliding panel probe and driving mechanism. The top plate was deliberately made very light so that the plate spacing could be varied easily by merely raising or lowering the upper plate. It was fabricated from a $\frac{1"}{32}$ Dural sheet mounted on a light plywood frame. The spacing between

two plates was maintained by wooden posts placed at the four corners; these seem to have little effect on the field distribution within, since the field strengths at the edges of the plates are relatively low. The plate separation could be varied by small distances with the help of thin plastic slabs placed on the supporting wooden posts. During the course of the experiment the plate spacing (antenna height) was varied from $\frac{1}{2}$" (0.04λ) to 12" (1.016λ). While examining the behavior of the antenna near resonance the plate spacing had sometimes to be varied by intervals as small as 0.3 cm (0.01λ). The plates were aligned by means of metal pins which fit through holes at the sides of the two plates so as to index the upper plate relative to the lower; after adjusting the plate spacing by means of the wooden corner posts, the metal pins were removed to avoid possible perturbing effects during the course of the measurements. The joints and screw slots on the surface of the plates were covered with strips of .001" aluminum foil with silver paint as adhesive. The two plates were carefully levelled to within 0.010 inch with the help of a theodolite and any unevenness noticed was corrected by placing suitable shims beneath the plates. Row (15) has investigated the effects of small variations in plate spacing and it is found that in practice, gradual departure from the ideal has very little effect on the performance, though sudden discontinuities may cause partial reflections. Bracewell (16) has found that the effect of these discontinuities is to introduce a shunt capacitance C_d (a) in the parallel-plate line whose magnitude is given by

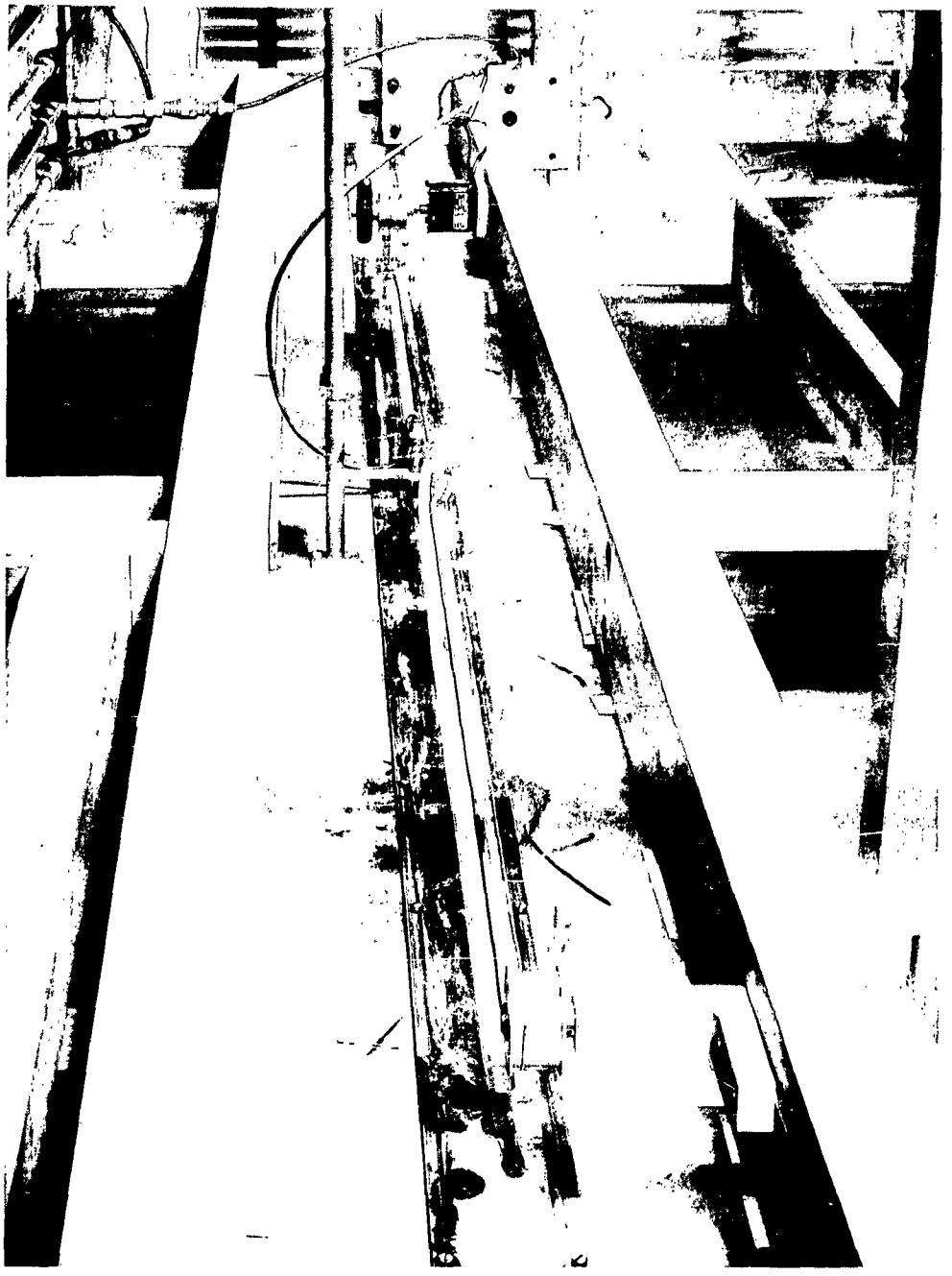

FIG. 1-22 SLIDING PANEL, PROBE AND DRIVING MECHANISM

$$C_d = \frac{2\mathcal{E}_o}{\pi^3} \sum_{1}^{\infty} \frac{\sin^2 n\pi a}{a^2 n^3}$$

where a is the ratio of the spacings (see Fig. 1-23)and $\mathcal{E}_o$ (.085 picofarads/meter) is the permittivity of free space. If the discontinuity is not large ($a \geq 0.9$) the discontinuity capacitance is only a minute fraction of a picofarad and does not cause noticeable perturbation. The other references which were helpful in designing the parallel-plate region were (17-20).

Absorbers

The wave propagating inside the parallel-plate region suffers a partial reflection at the edges because of the discontinuity in impedance. The theoretical value of the reflection coefficient as a function of plate spacing has been calculated by Marcuvitz (21) and is plotted in Fig. 1-24 . It can be seen that strong reflections occur for close plate spacing which can seriously affect the measured value of the admittance of the antenna. In order to eliminate the reflection it was necessary to terminate the rims of the parallel plate with absorbing wedges. The wedges had to be sufficiently thin (approximately 1 cm) so that the plate separation could be varied in small intervals in order to study the behavior of the antenna admittance as a function of its length. Commercially available L-band absorbers, besides being prohibitively expensive, were also far too large to be suitable for the purpose of this experiment. It was therefore decided

to make the absorbers in the laboratory itself from linearly tapered polyfoam wedges coated with an energy dissipating substance like carbon black or graphite. The two determining factors (22) in the design of these 'gradual transition' type absorbers are (1) the length of the transition, (2) the optimum layer thickness of the absorbing substance. The lower frequency limit is given by the length of the wedges. Halford (23) has shown that the reflection coefficient of such wedges varies periodically with their length as shown in Fig. 1.25. There appears to be no clear-cut upper limiting frequency, though in the case of acoustic absorbers (24), it is found that the reflection rises at higher frequencies when separation between the individual wedges becomes too large. Because of its low dielectric constant and the ease with which it could be cut and tapered the wedges were made from $\frac{1}{2}$-inch thick polyfoam sheet and were tapered for 1 wavelength (11 3/4 inches). The separation between the individual wedges was approximately 5 cm ($\frac{1}{6}$ λ) and the total length of each wafer was 4 $\frac{1}{2}$ feet. Thin plywood strips provided with wooden screws were glued to the base of these wedges. The wedges were then sprayed with 3-E-14D Black No. 1 -- a colloidal dispersion of carbon black in liquid Neoprene, a product manufactured by the General Latex and Chemical Co., Cambridge, Mass. The whole wafer thus assembled (see Fig. 1.26) could be inserted inside the parallel-plate region and screwed onto slotted wooden panels placed at the edges of the parallel plates. The plate

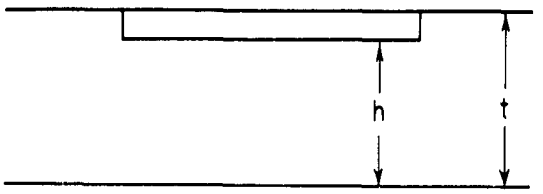

Ratio of Spacings $\alpha = h/t$

FIG. 1-23. Discontinuity in Parallel-Plate Region
(From Reference 16)

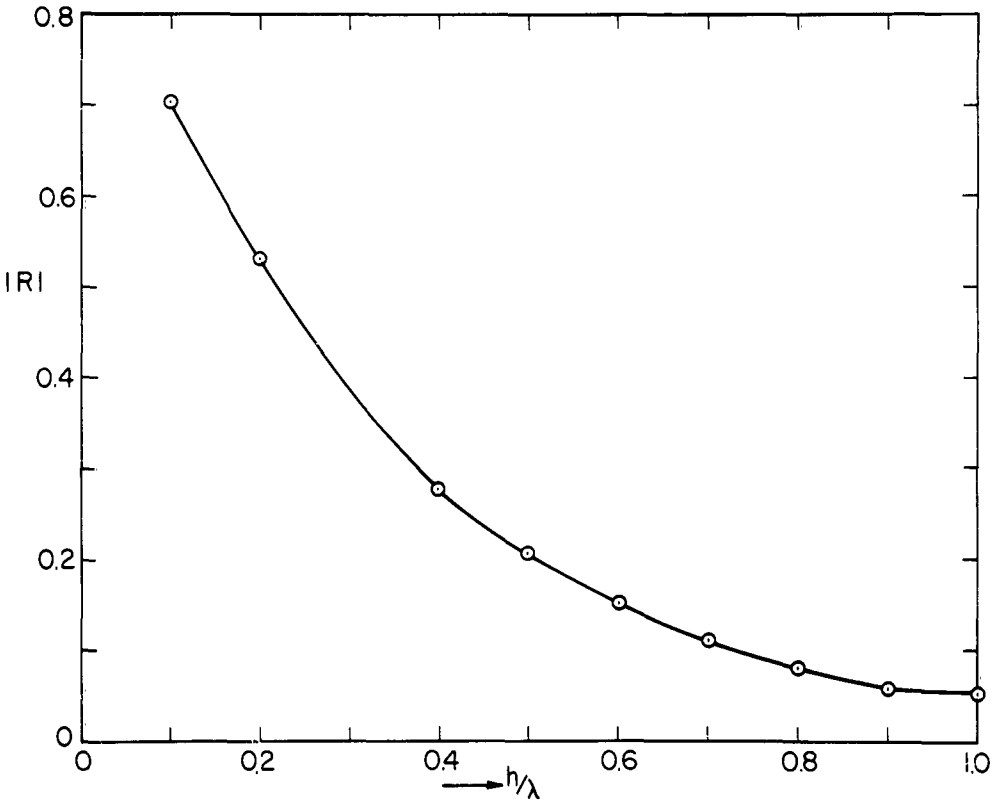

FIG. 1-24 REFLECTION COEFFICIENT OF THE EDGE OF THE PARALLEL-PLATE REGION

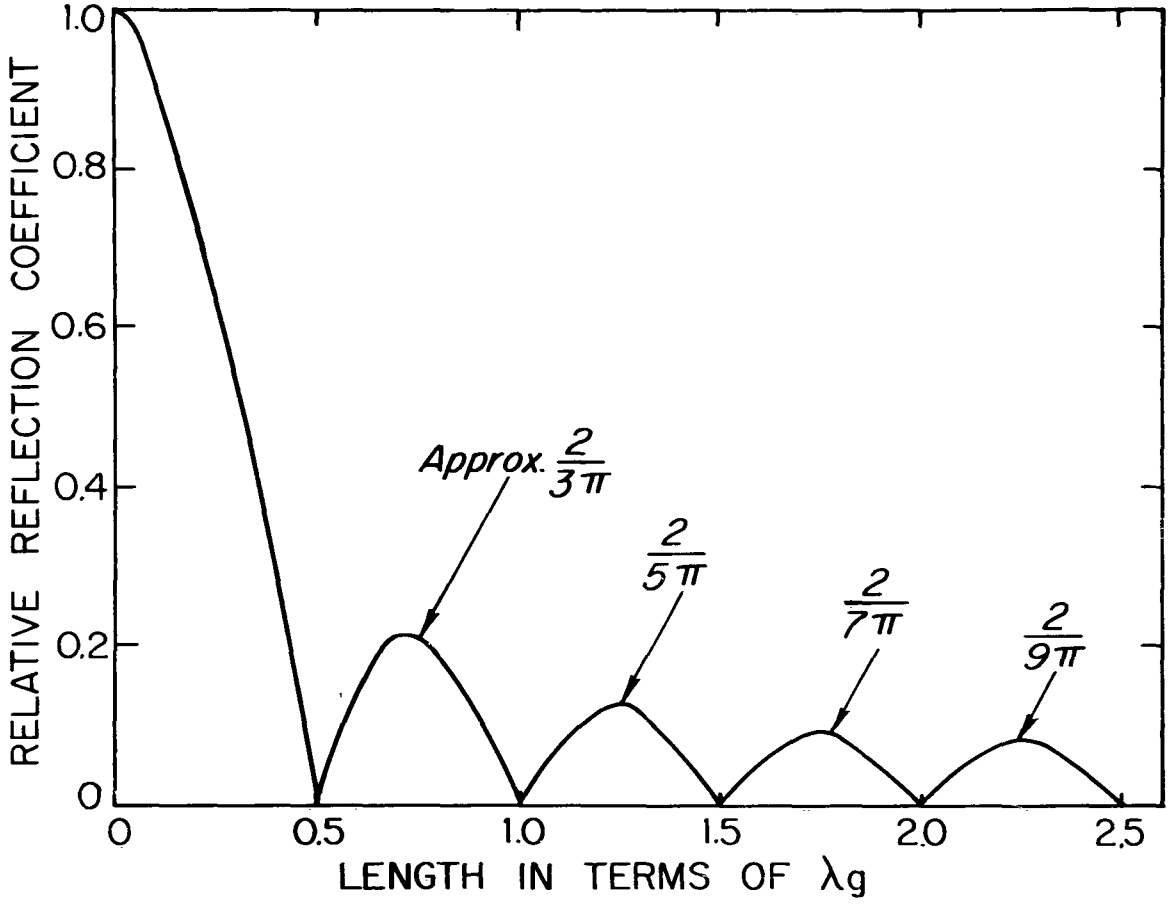

FIG. 1-25 VARIATION OF REFLECTION COEFFICIENT WITH LENGTH FOR LINEAR TAPER. *(FROM REF. 23)*

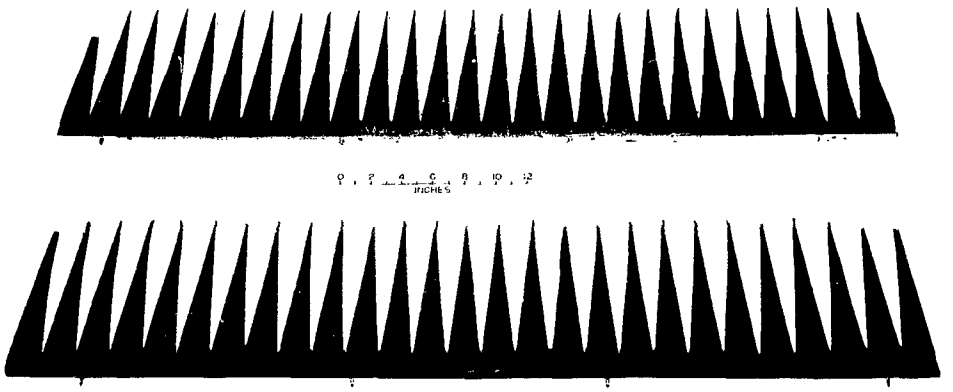

FIG. 1-26 ABSORBING WEDGES

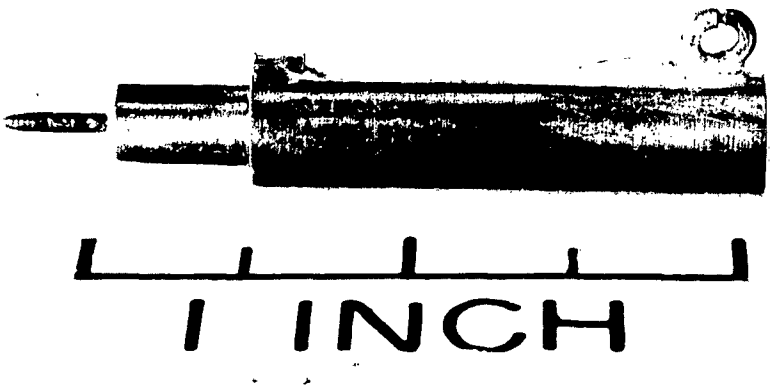

FIG. 1-27 SHIELDED LOOP CURRENT PROBE

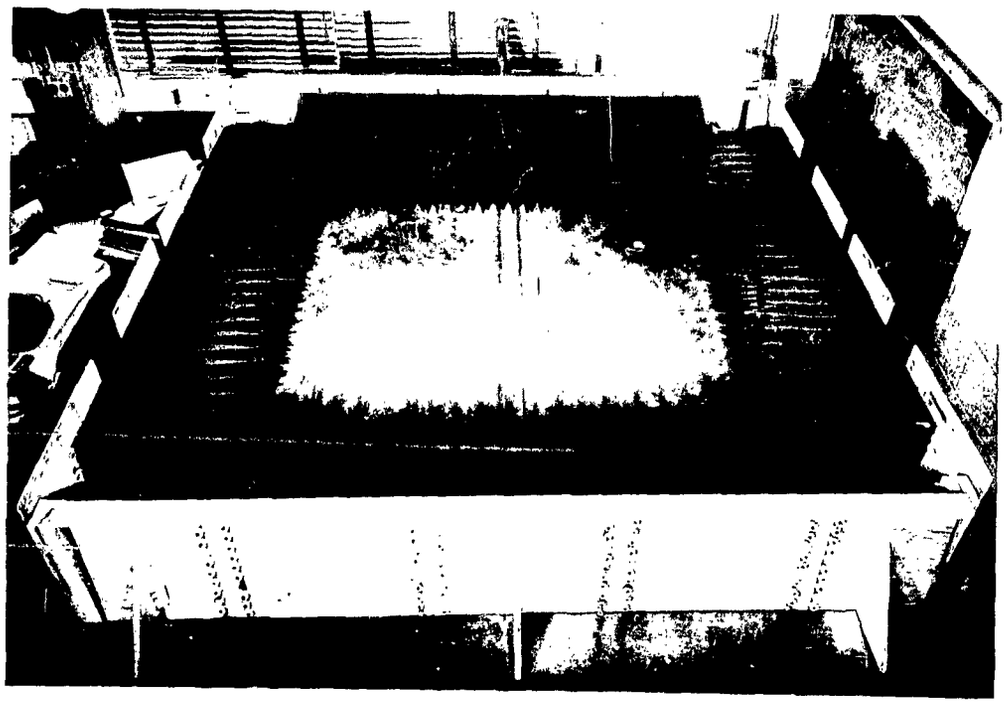

FIG. 1-28 PARALLEL-PLATE REGION WITH TOP-PLATE REMOVED

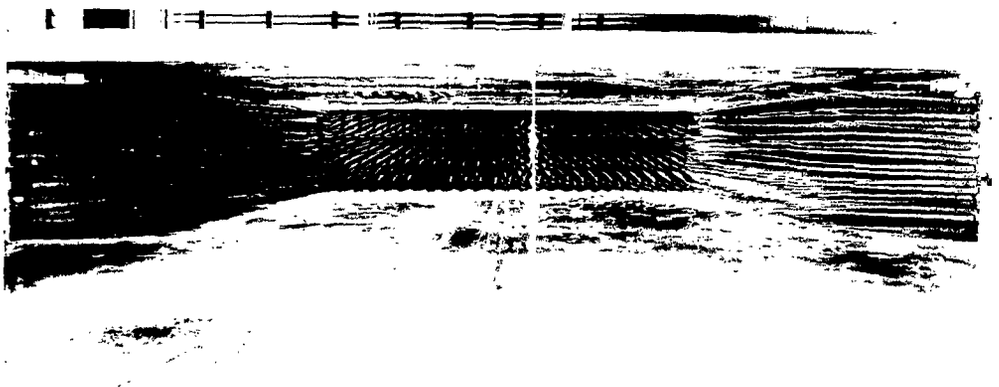

FIG. 1-29 SIDE VIEW OF PARALLEL-PLATE REGION

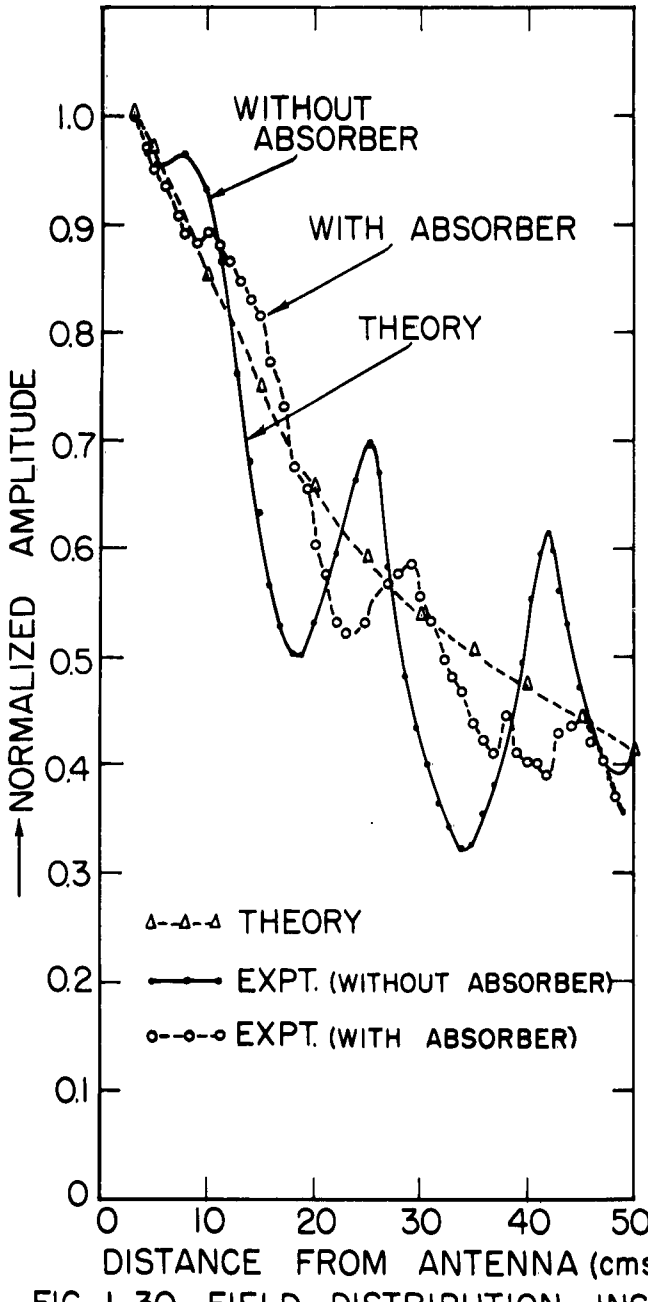

FIG. 1-30 FIELD DISTRIBUTION INSIDE PARALLEL-PLATE REGION WITH & WITHOUT ABSORBERS
$k_0 h = 0.5319$

separation could be easily varied by removing or adding each wafer in turn. Fig. 1.28 shows a picture of the parallel-plate region with the top plate removed; the absorbers mounted on wooden panels, the antenna and the sliding panel with probe for measuring the standing-wave ratio in the guide can all be seen in the picture. Fig. 1.29 gives a side view of the same arrangement with the top plate in place.

The favorable layer thickness of the carbon black mixture was determined by giving the wedges various coatings and determining the standing-wave ratio in each case. Fig. 1.30 gives the normalized field distribution inside the parallel-plate region with and without the absorbing wedges for a plate separation of $h/\lambda = 0.084$. The standing-wave ratio without absorbers was 1.72 at a distance of about 25 cm from the antenna. After the insertion of the absorbing wedges with about 4 coatings of the carbon black mixture the SWR was brought down to about 1.12. No appreciable reduction in SWR was noticed by increasing the number of coatings on the wedges. The normal component of the electric field in the parallel-plate guide is given by $E_z = cH_o^{(2)}(k_o r)$ where $k_o = 2\pi/\lambda$. This has also been plotted in Fig. 1.30 for the sake of comparison. It can be seen from Fig. 1.24 that the edge reflections become less pronounced as the plate separation increases. This fact was also confirmed experimentally. For large spacings the SWR fell to less than 1.07. However, when the plate separation was a half-wavelength a sudden increase in SWR was noticed.

The reflection coefficient calculated from Marcuvitz's admittance values does not account for this phenomenon. After inserting the absorbers, however, the SWR was once again brought down to a reasonable level.

Measuring Techniques

The experimental techniques for measuring the impedance and current distribution of the antenna have become fairly standardized, thanks to the efforts of the previous research workers in this laboratory.

The coaxial measuring line was quite similar to the one devised by T. Morita (25); a schematic sketch of the line is given in Fig. 1.31. The measuring line was installed vertically beneath the parallel-plate region. In order to reduce the end effects and the possible effect that the aperture of the coaxial line might have on the multiple series of images, the ratio of the diameters of the outer to the inner conductor was chosen to be 2.25. The center conductor of the coaxial line was $\frac{1"}{4}$ diameter brass tubing; it could be extended from 0 to 32 cm above the lower ground screen by means of a rack and pinion arrangement. The inner conductor had a $\frac{1"}{16}$ slot along its entire length, through which the shielded probe could travel. The probe was mounted on a $\frac{3"}{16}$ brass tube which slid inside the center conductor and was positioned by another rack and pinion arrangement. Both the probe and antenna could be positioned to 0.1 mm by means of a steel scale and vernier. The signal from the probe to the detector was carried by a microdot cable. The coaxial line was driven by means of a T-shaped stub, connected to the main line at a distance of $\lambda/4$ from the short-circuited end. The probe was small shielded loop, approximately 2.5 mm

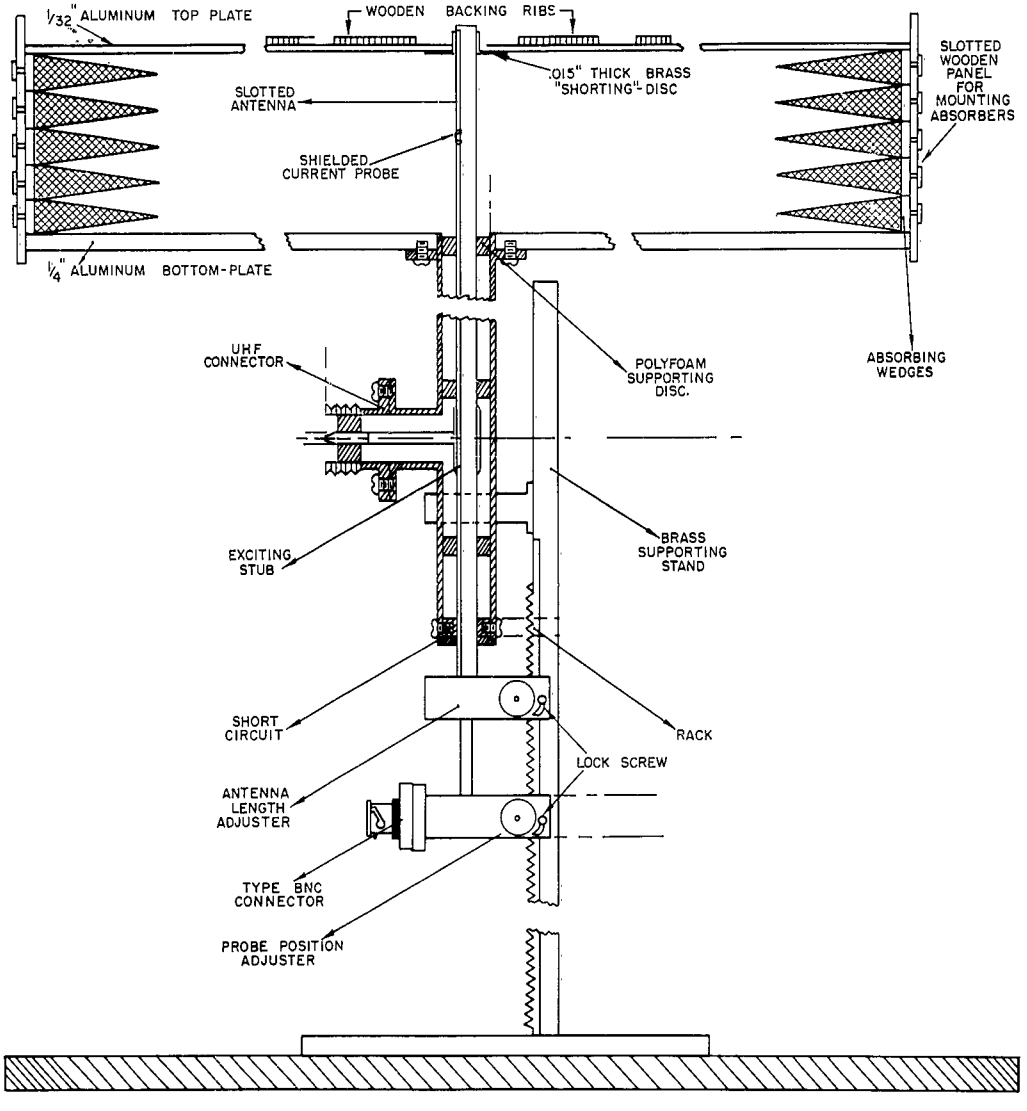

FIG. 1-31 SKETCH OF MEASURING LINE AND PARALLEL-PLATE REGION

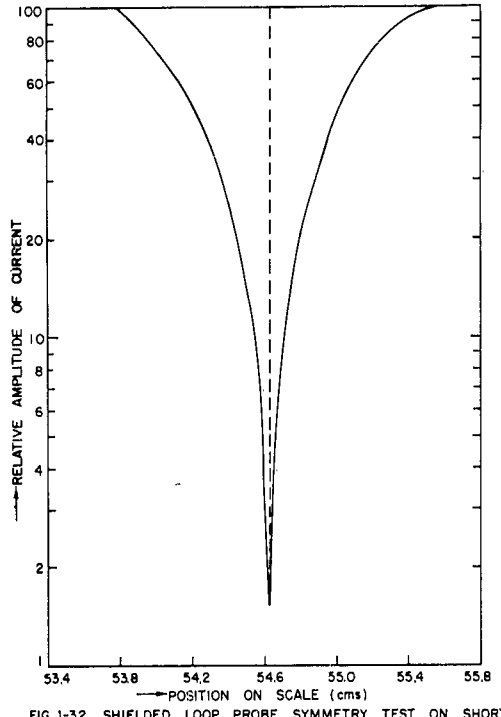

FIG. 1-32 SHIELDED LOOP PROBE SYMMETRY TEST ON SHORT CIRCUITED LINE.

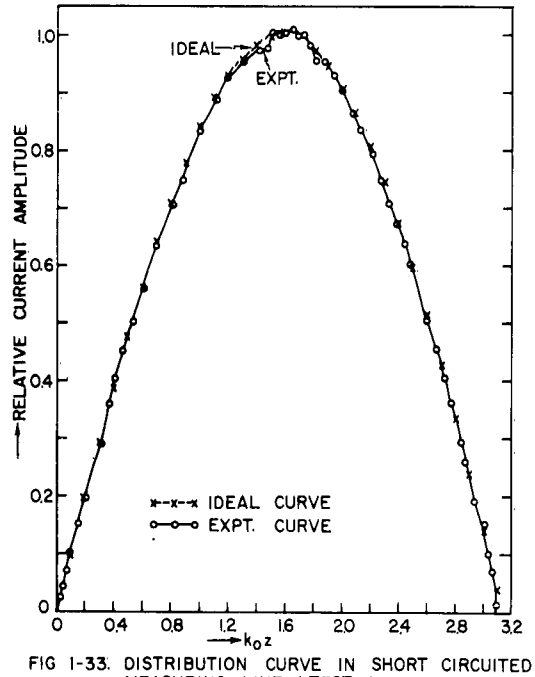

FIG 1-33. DISTRIBUTION CURVE IN SHORT CIRCUITED MEASURING LINE. (TEST FOR PROBE LOADING)

(0.008λ) in diameter; it was made from .021" O.D. x .003" wall precision coaxitube. (See Fig. 1.27). Since the frequency of 1000 Mc used in these experiments is considerably higher than frequencies hitherto used in this laboratory for antenna measurements of this nature, a comprehensive series of tests was made to determine the accuracy of the measuring equipment. Particular attention was focused on the preparation of the probe which usually causes the greatest errors. Care was taken to construct the probe symmetrically, since in the vicinity of a current minimum, slight asymmetries can introduce sizeable errors. That the final probe is well-balanced is shown by the symmetry of the distribution curve near a current minimum. (Fig. 1.32). In order to determine the possible perturbing effect of the probe, the coaxial line was short-circuited and the experimentally measured current distribution curve inside the line was compared with an ideal sinusoidal distribution. As can be seen from Fig. 1.33 the probe does cause slight perturbation at the peak of the curve, but the effect does not appear to be significant enough to cause appreciable errors. The input impedance of a free-space monopole as measured with the present experimental set-up compared favorably with the values obtained by Hartig (27). The constants of the measuring line are listed below:

Inner radius of outer conductor b = 9/32 inch.

Outer radius of antenna a = 1/8 inch.

$$b/a = 2.25$$

Characteristic admittance of line = Y_c = 20.57 mhos.

Characteristic impedance Z_c = 48.6 ohms.

Frequency of measurement = 1000 Mc.

Wavelength in air = 30 cm.

Wavelength in line = 28.9 cm..

Capacitive end-correction = $B_T = \omega C_T$ = -0.584 millimhos.

Apparatus

A superheterodyne detecting system was used in the experiment. The signal generator used in the experiment was a General Radio Type 1218-A Unit Oscillator having a frequency range of 900-2000 Mc. and a maximum power output of 200 MW. Higher harmonics generated by the oscillator were suppressed by a GR Type 874-F1000 low-pass filter with a cut-off frequency of 1000 Mc. (+ 10 %). To avoid frequency pulling the oscillator was isolated from the rest of the circuit by a 20 db attenuating pad. The detecting system consists of a General Radio Type 1216 A-I. F. Amplifier used in conjunction with a GR Type 874-MR mixer rectifier with a type 1-N21B crystal diode. The local oscillator was another GR Type 1218-A Unit Oscillator. The I. F. amplifier is provided with a 70 db precision step attenuator with an accuracy of $\pm$ 0.3 db + 1 %; good linearity is obtained over the whole range of the instrument. The amplifier was calibrated by using the sinusoidal voltage distribution in a short-circuited coaxial line as a reference. The calibration curve is shown in Fig. 1.34.

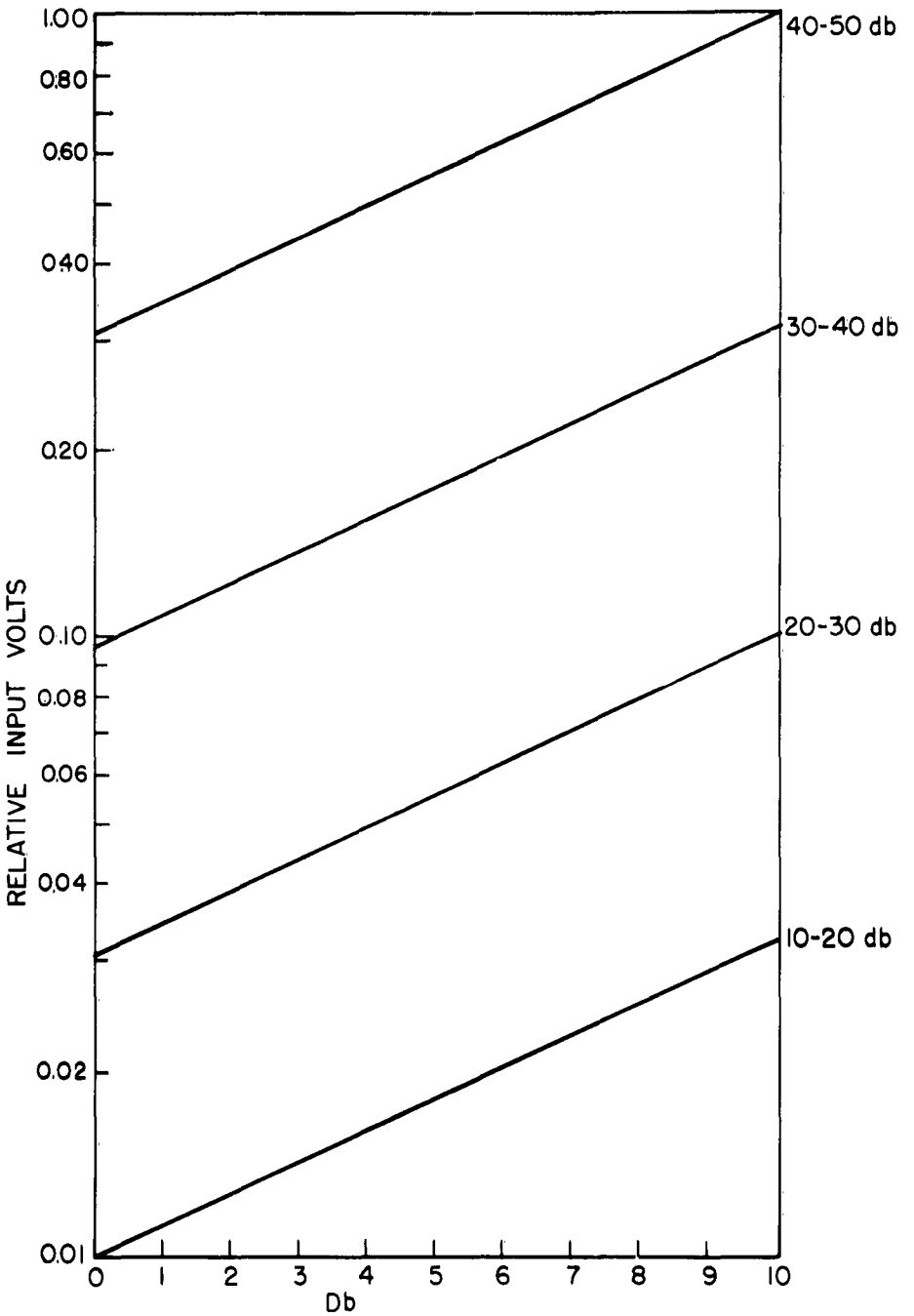

FIG. 1-34 CALIBRATION CHART: G. R. UNIT AMPLIFIER TYPE 1216-A #2410 CRYSTAL-MIXER; 874 MR; FCY: 1000 MC.

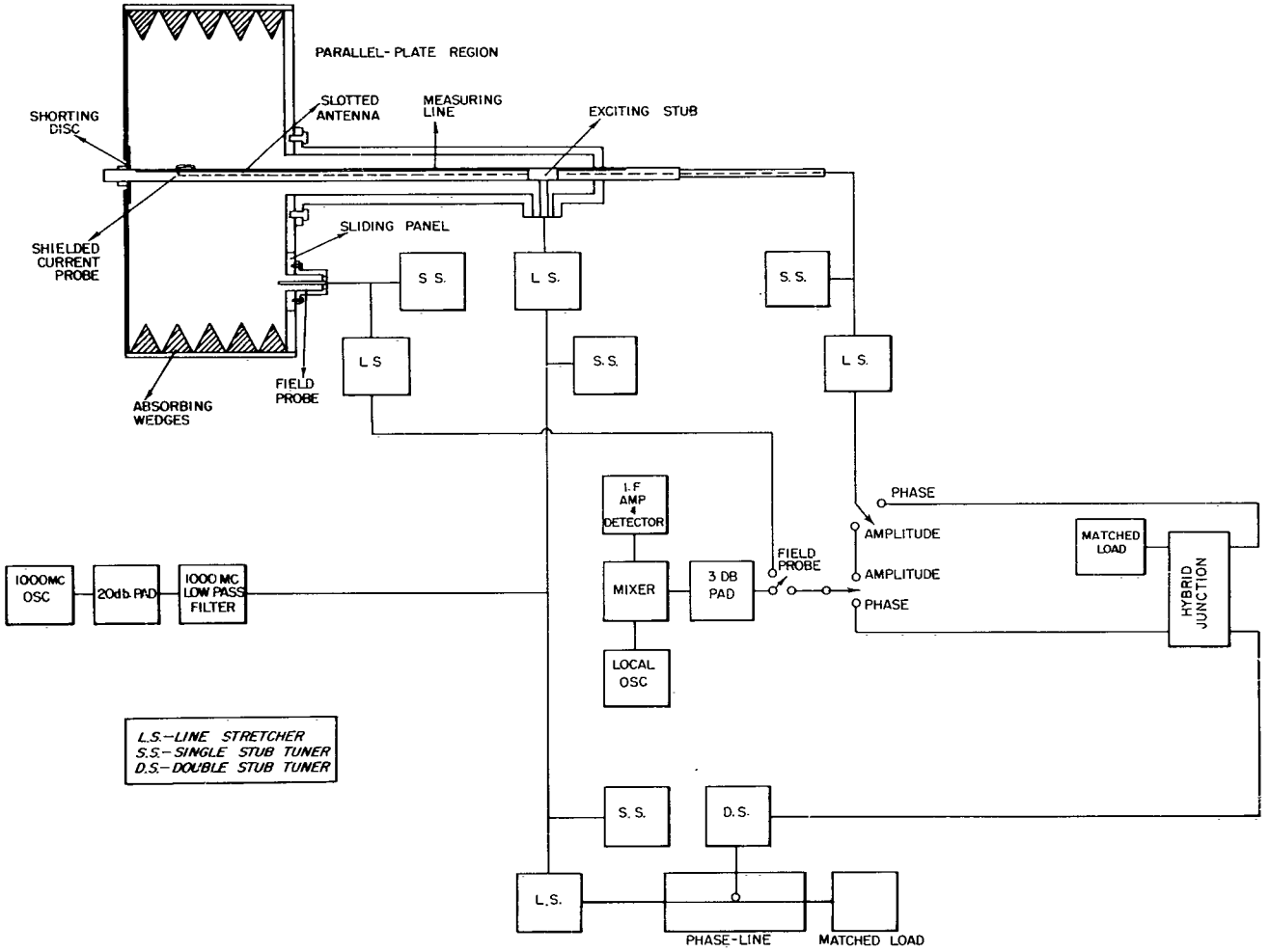

FIG. I-35 BLOCK DIAGRAM OF EXPERIMENTAL EQUIPMENT

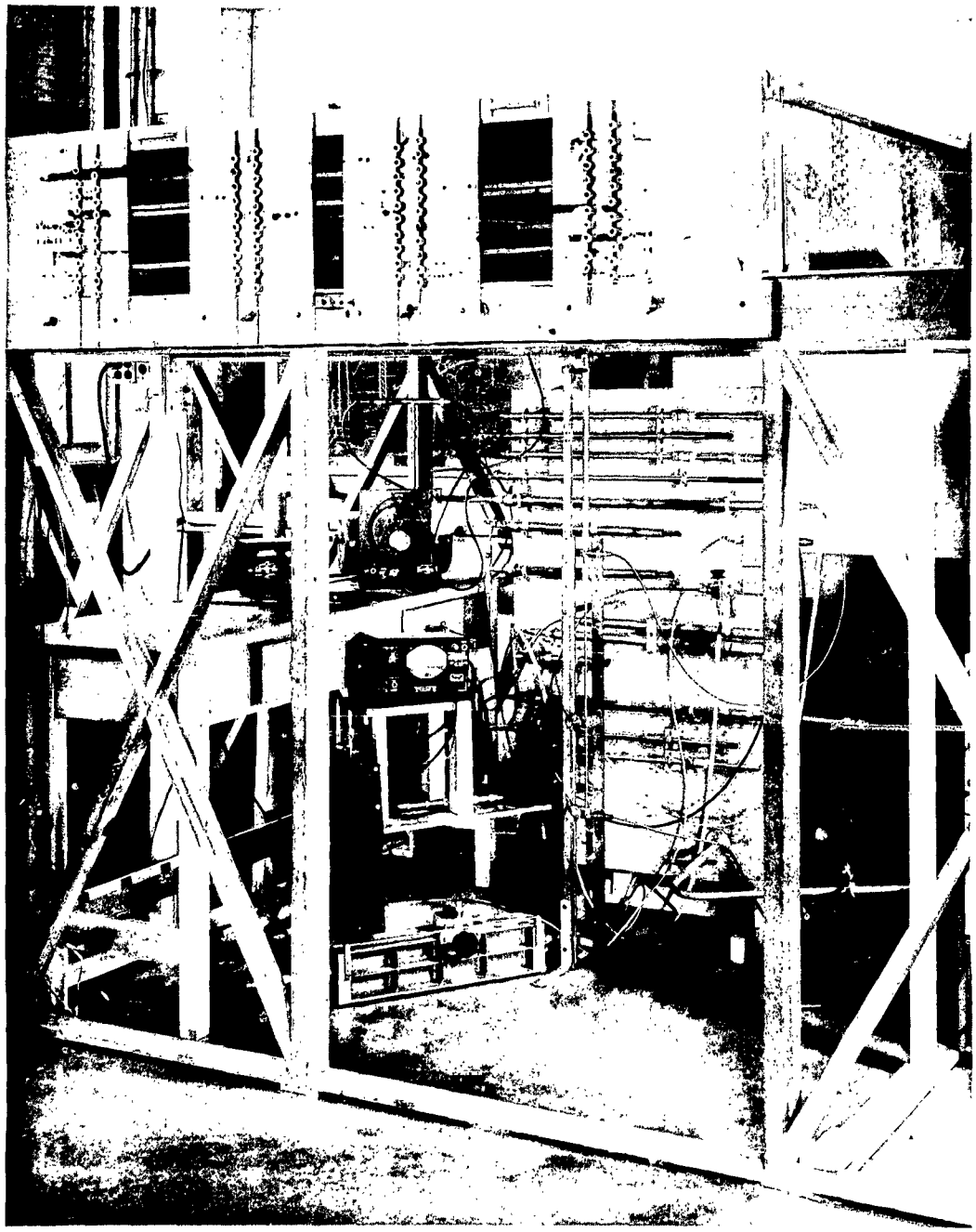

FIG. 1-36 MEASURING APPARATUS

A schematic sketch of the experimental layout is shown in Fig. 1.35. Figure 1.36 gives a pictorial view of the apparatus.

Current Distribution

The current distribution on the antenna can be completely described by measuring the relative amplitude and phase. The amplitude can be measured quite easily by connecting the probe output directly to the detecting system through a tuning network.

In order to measure the relative phase, the signal from the probe is compared with a reference signal obtained from a non-resonant slotted line terminated in its characteristic impedance. The phase line used in the experiment was a Hewlett-Packard Model 805A slab line terminated by a GR Type 874 WM 50 ohm termination; the standing-wave ratio on the line was less than 1.05. The probe and the reference signals are mixed in by a coaxial hybrid junction (Narda Model No. 3032). The difference arm of the hybrid was connected to the detecting system. By adjusting the phase and amplitude of the reference signal from the phase line a maximum indication could be obtained, signifying that the two signals are 180° out of phase. After establishing such a reference point, the phase at other points along the antenna could be determined with respect to it by simply noting the distance between the minimum settings of the probe in the phase line.

Admittance Measurement

Two techniques were employed to measure the input admittance of the antenna. At low VSWR the ratio of maximum to minimum current was measured directly and the terminal function ρ_s of the antenna load was calculated from the formula

$$\rho_{sa} = \coth^{-1} S$$

where S = current standing-wave ratio. At higher VSWR the terminal function was determined by the distribution curve (double minimum) method. If $\Delta\ \omega$ is the distance between half-power points, the apparent terminal function is given by

$$\rho_{sa} = \beta \frac{\Delta\omega}{2} \qquad \text{where } \beta = \frac{2\pi}{\lambda g}$$

where λg is the wavelength in the coaxial line.

The apparent phase function can be found from the equation

$$\Phi_{sa} = \frac{\pi}{2} + \beta\ (\omega_1 - \omega_2)$$

where ω_1 is the position of the current minimum with a short-circuit terminating the line and ω_2 is the current minimum with the antenna load. The input admittance may then be calculated from the formulas.

$$\frac{G}{Y_c} = \frac{\sinh 2\rho}{\cosh 2\rho + \cos 2\Phi}$$

$$B/Y_c = \frac{\sin 2\Phi}{\cosh 2\rho + \cos 2\Phi}$$

and $Y_a = G + jB$; Y_c = charge admittance of line .

End Correction

The ideal or theoretical antenna admittance Y_o may be obtained from the corresponding measured apparent admittance Y_a by noting that

$$Y_a = Y_o + j\omega C_T$$

where C_T is a lumped terminal zone capacitance that takes account of end and coupling effects near the end of the measuring line. C_T has been evaluated approximately (26) and is given by

$$C_T = - f(b/a)\, c_o b$$

where $c_o = 2\pi \mathcal{E}_o / \ln(b/a)$ is the capacitance per unit length of the line, a is the antenna radius and b is the inner radius of the outer conductor of the coaxial line.

The function $f(\frac{b}{a}) = - C_T/c_o b$ has been given in (26). For $b/a = 2.25$, $- C_T/c_o b = 0.18937$. The corresponding end-correction is $-j\omega C_T = - 0.5839 \times 10^{-3}$ mhos . The end-correction in (26) is for $a/\lambda = 3.9 \times 10^{-3}$. The correction to be applied to the experimental results is likely to be slightly larger since $a/\lambda = 10.05 \times 10^{-3}$. However, this difference in correction term is almost negligible, particularly since the capacitance end-correction is very small and can be virtually ignored except in the vicinity of resonance and antiresonance.

ACKNOWLEDGMENT

The author is deeply grateful to Professor R. W. P. King for suggesting the problem and for his constant encouragement and guidance throughout the course of this investigation. He also wishes to thank Prof. T. T. Wu, Dr. D. F. Winter, Dr. J. M. Myers, and Mr. A. K. Rajagopal for helpful discussions. Acknowledgement is also due Messrs. E. J. Johnson and J. C. Meehan for their meticulous machine work and help in the design and construction of the experimental equipment; to Mr. Donald J. Macmillan for constructing the subminiature probe which contributed largely to the success of this research; and to Mr. J. K. Yuh and Miss Ruth Edelson for carrying out the laborious numerical computations.

REFERENCES

1. R. W. P. King, The Theory of Linear Antennas, Harvard University Press, 1956.

2. L. Infeld, A. F. Stevenson, and J. L. Synge, "Contributions to the Theory of Waveguides", Canadian Journal of Research, Vol. 27, pp. 68-129, July 1949.

3. L. Lewin, "A Contribution to the Theory of Cylindrical Antennas - Radiation between Parallel-Plates", IRE Trans. on Antennas and Propagation, Vol. AP-7, pp. 162-168, April 1959.

4. L. Lewin, "A Contribution to the Theory of Probes in Waveguides", Proc. Inst. of Elec. Engrs., Vol. 105, Part C, pp. 109-116, 1958.

5. W. Magnus and F. Oberhettinger, Formulas and Theorems for the Functions of Mathematical Physics, Chelsea Publishing Col 1954.

6. T. T. Wu, "Input Admittance of Linear Antennas Driven from a Coaxial-Line", Cruft Lab. Tech. Report No. 357, p. 11, 1962.

7. T. T. Wu and R. W. P. King, "Driving-Point and Input Admittance of Linear Antennas", Journal of Applied Physics, Vol. 30, No. 1, pp. 74-76, January 1959.

8. R. H. Duncan, "Theory of the Infinite Cylindrical Antenna Including the Feedpoint Singularity in Antenna Current", Journal of Research of the National Bureau of Standards, Vol. 66D, No. 2, March-April 1962.

9. Y. M. Chen and J. B. Keller, "Current on and Input Impedance of a Cylindrical Antenna", Report from the Institute of Mathematical Sciences, New York University, N. Y., July 1961.

10. R. H. Duncan and F. A. Hinchey, "Cylindrical Antenna Theory", Journal of Research of the National Bureau of Standards -- D. Radio and Propagation, Vol. 64D, No. 5, Sept.-Oct. 1960.

11. J. E. Storer, "Variational Solution to the Problem of the Symmetrical Cylindrical Antenna", Cruft Lab. Tech. Report No. 101, Feb. 1950.

12. E. Jahnke and F. Emde, Tables of Functions (6th Edition, Dover Publications, pp. 37-41.

13. A. S. Meier and W. P. Summers, "Measured Impedance of Vertical Antenna over Finite Ground Plane", Proc. IRE, Vol. 37, pp. 609-616, June 1949.

14. H. W. Andrews, " Image Plane and Coaxial-Line Measuring Equipment at 600 Mcs.", Cruft Lab. Tech. Report No. 177, Harvard University, July 1953.

15. R. V. Row, "Microwave Diffraction Measurements in a Parallel-Plate Region", Cruft Lab. Tech. Report No. 153, May 1952.

16. R. N. Bracewell, "Step Discontinuities in Disk Transmission Lines", Proc. IRE, Vol. 42, p. 1543, 1954.

17. J. E. Keys, "A Parallel-Plate Region for Microwave Measurements at 10 cm", Project Report No. 5-0-1, Sept. 1955. Defense Research Telecommunication Establishment, Ottawa, Canada.

18. R. Plonsey, "Diffraction by Cylindrical Reflectors", Proc. Inst. Elec. Engrs., Vol. 105, Part C, p. 312, 1958.

19. M. M. J. El-Kharadly, "Some Experiments on Artificial Dielectrics at Centimetre Wavelengths", Proc. Inst. of Elec. Engrs., Vol. 103B, p. 419, May 1956.

20. P. H. Sollom and J. Brown, "A Centimetre Wave Parallel-Plate Spectrometer", Proc. Inst. of Elec. Engrs., Vol. 103B, p. 419, May 1956.

21. N. Marcuvitz, Wave Guide Handbook, M. I. T. Radiation Laboratory Series, Vol. 10, p. 179-181, McGraw-Hill.

22. E. Meyer and R. Pottel, "Low Reflection Absorbers of Electromagnetic Waves", Air Force Cambridge Research Lab. Report ARCRL-TR-60-199. (Project 4610 Task 46102), November 1960.

23. G. H. Halford, Proc. Inst. Elec. Engrs., Vol. 100, p. 117, 1953.

24. E. G. Richardson, "Technical Aspects of Sound", Vol. II, Chap. 6, Sec. 5, p. 271, Elsevier Publishing Company, 1957.

25. T. Morita, "Measurements of Current and Charge Distribution on Cylindrical Antennas", Cruft Lab. Tech. Report No. 66, 1949.

26. R. W. P. King, "Theory of Linear Antennas", Chap. II, Fig. 38-19, p. 251, Harvard University Press, 1956.

27. E. O. Hartig, "Circular Apertures and their Effects on Half-dipole Impedances", Cruft Lab. Tech. Report No. 107, June 1950.

APPENDIX - I

Equation 1.28 may be rigorously derived in the following manner.

Consider the integral

$$Q = \int_0^{\pi} K_o (j2k_o a \sin\theta)\, d\theta \quad . \tag{1.28}$$

From the identity

$$K_o (j2k_o a \sin\theta) = -j\pi/2\ H_o^{(2)} [2k_o a \sin\theta]$$

it follows that

$$Q = -j\pi/2 \int_0^{\pi} H_o^{(2)}[c \sin\theta]\, d\theta = -j\ /2 \left[\int_0^{\pi} J_o (c \sin\theta)\, d\theta - j \int_0^{\pi} N_o (c \sin\theta)\, d\theta \right]$$

where $c = 2k_o a$. (1.96)

Using the formula

$$J_n^{\,2} (z) = \frac{1}{\pi} \int_0^{\pi} J_o (2z \sin\phi) \cos 2n\phi\ d\phi \text{ for } n = 0, 1, 2 \ldots$$

we have

$$\int_0^{\pi} J_o (c \sin\theta)\, d\theta = \pi\ J_o^{\,2} (c/2) \quad . \tag{1.97}$$

Consider now the integral

$$\int_0^{\pi} N_o (c \sin\theta)\, d\theta$$

The integral representation for the N function is given by 5[M and O, p. 27]

$$N_\nu(x) = -\frac{2(\frac{1}{2}x)^\nu}{\Gamma(\frac{1}{2}-\nu)\,\Gamma(\frac{1}{2})} \cdot \int_1^\infty \frac{\cos xt}{(t^2-1)^{\nu+\frac{1}{2}}}\,dt$$

for $-1/2 < \mathrm{Re}\,\nu < \frac{1}{2}$; x real and positive.

When $\nu = 0$ we have

$$\int_0^\pi N_o(c\sin\theta)\,d\theta = -2/\pi \int_0^\pi \int_1^\infty \frac{\cos(c\sin\theta)\,t}{\sqrt{t^2-1}}\,dt\,d\theta$$

$$= -2/\pi \int_1^\infty \frac{dt}{\sqrt{t^2-1}} \int_0^\pi \cos(ct\sin\theta)\,d\theta\,. \qquad (1.98)$$

Since

$$\int_0^\pi \cos(ct\sin\theta)\,d\theta = \pi\, J_o(ct)\,,$$

$$\int_1^\pi N_o(c\sin\theta)\,d\theta = -2\int_1^\infty \frac{J_o(ct)}{\sqrt{t^2-1}}\,dt\,. \qquad (1.99)$$

Making the substitution $t = \sqrt{\rho^2+1}$, we have

$$\int_1^\infty \frac{J_o(ct)}{\sqrt{t^2-1}}\,dt = \int_0^\infty \frac{J_o(c\sqrt{\rho^2+1})}{\sqrt{\rho^2+1}}\,d\rho\,. \qquad (1.100)$$

Using another identity given by (5)

$$J_{\nu/2}(x/2)\, N_{\nu/2}(x/2) = -2/\pi \int_0^\infty \frac{J_\nu(x\sqrt{t^2+1})}{\sqrt{t^2+1}}\, dt$$

(Re ν >-1, x real and positive)

we have for $\nu = 0$

$$\int_0^\infty \frac{J_o(x\sqrt{t^2+1})}{\sqrt{t^2+1}}\, dt = -\pi/2\ J_o(x/2)\ N_o(x/2) \quad . \tag{1.101}$$

Using 1.100 and 1.101 in 1.99

$$\int_0^\pi N_o(c \sin\theta)\, d\theta = \pi\ J_o(c/2)\ N_o(c/2) \tag{1.102}$$

Substituting 1.97 , 1.102 in 1.96 we obtain

$$Q = \int_0^\pi K_o(j2k_o a \sin\theta) = -j\pi^2/2\ J_o(k_o a)\ H_o^{(2)}(k_o a) \quad . \tag{1.28}$$

Air Force List A*

AFMTC
(AFMTC Tech Library-MU-135)
Patrick AFB, Florida

OAR(RROS, Col. John R. Fowler)
Tempo D
4th and Independence Ave.
Washington 25, D. C.

ASD (ASAPRD-Dist)
Wright-Patterson AFB, Ohio

AF Missile Development Center
(MDGRT)
Holloman AFB, New Mexico

Commanding General, USASDRL
Fort Monmouth, New Jersey
Attn: Tech. Doc. Ctr.
SIGRA/SL-ADT

Commanding Officer
Attn: ORDTL-012
Diamond Ordnance Fuze Laboratories
Washington 25, D. C.

Office of Scientific Intelligence
Central Intelligence Agency
2430 E Street, N.W.
Washington 25, D. C.

Scientific and Technical
Information Facility
Attn: NASA Representative
(S-AK/DL)
P.O. Box 5700
Bethesda, Maryland

Director (Code 2027) [2]
U. S. Naval Research Laboratory
Washington 25, D. C.

AFCRL, OAR(CRXRA-Stop 39)
L. G. Hanscom Field [10]†
Bedford, Massachusetts

Technical Information Office
European Office
Aerospace Research
Shell Building, 47 Cantersteen
Brussels, Belgium

Office of Naval Research
Branch Office
London
Navy 100, Box 39
F. P. O., New York, New York

Massachusetts Institute of
Technology
Research Laboratory
Building 26, Room 327
Cambridge 39, Massachusetts
Attn: John H. Hewitt

AUL
Maxwell AFB, Alabama

AFOSR, OAR (SRYP)
Tempo D
4th and Independence Ave.
Washington 25, D. C.

RADC (RAALD)
Griffiss AFB, New York
Attn: Documents Library

Hq. OAR
(RROSP, Major Richard W. Nelson)
Washington 25, D. C.

Department of the Army
Office of the Chief Signal Officer
Washington 25, D. C.
Attn: SIGRD-4a-2

Redstone Scientific Information Center
U. S. Army Missile Command
Redstone Arsenal, Alabama

DDC (TIPPAA) [10]
Arlington Hall Station
Arlington 12, Virginia

Director
Langley Research Center
National Aeronautics and
Space Administration
Langley Field, Virginia

Chief, Bureau of Naval Weapons [2]
Department of the Navy
Attn: DLI-31
Washington 25, D. C.

Director, USAF Project RAND
The Rand Corporation
1700 Main Street
Santa Monica, California
THRU: AF Liason Office

Library
Boulder Laboratories
National Bureau of Standards
Boulder, Colorado

Aero Res. Lab. (OAR)
AROL Lib. AFL 2292, Bld. 450
Wright-Patterson AFB, Ohio

Defense Research Member
Canadian Joint Staff
2450 Massachusetts Avenue, N.W.
Washington 8, D. C.

U.S. Army Aviation Human Research Unit
U.S. Continental Army Command
P.O. Box 428, Fort Rucker, Alabama
Attn: Maj. Arne H. Eliasson

- - - - - - -

*One copy, unless otherwise specified by numbers enclosed in brackets.

†Mail separately from any other reports going to this Hqs.

Air Force List K*

ASD(ASRNRE-3, Mr. Paul Springer)
Wright-Patterson AFB
Ohio

Director
U. S. Army Ordnance
Ballistic Research Laboratories
Aberdeen Proving Ground
Maryland
Attn: Ballistic Measurements Lab.

Stanford Research Institute [2]
Menlo Park, California
Attn: Dr. D. R. Scheuch, Asst. Dir.
Division of Engineering Research

Goodyear Aircraft Corporation
1210 Massillon Road
Akron 15, Ohio
Attn: Library, Plant G

Convair, A Division of
General Dynamics Corporation
3165 Pacific Highway
San Diego 12, California
Attn: Mr. R. E. Honer
Head Electronics Research

Chu Associates
P. O. Box 387
Whitcomb Avenue
Littleton, Massachusetts

General Electric Company
Building 3, Room 143-1
Electronics Park
Syracuse, New York
Attn: Yolanda Burke
Documents Library

AFCRL, OAR
L. G. Hanscom Field
Bedford, Massachusetts
Attn: CRRD: Carlyle J. Sletten [3]
CRRD: Contract Files [2]
CRRD: Robert A. Shore [6]

Chief of Naval Operation
Department of the Navy
Attn: OP-413-B21
Washington 25, D. C.

Commander
U. S. Naval Air Missile Test Center
Point Mugu, California
Attn: Code 366

University of California
Department of Engineering
Berkeley 4, California
Attn: Antenna Laboratory

Cornell University
School of Electrical Engineering
Ithaca, New York
Attn: Prof. G. C. Dalman

The Johns Hopkins University
Radiation Laboratory [2]
1315 St. Paul Street
Baltimore, Maryland

The Johns Hopkins University
Applied Physics Laboratory [2]
8621 Georgia Avenue
Silver Springs, Maryland

McGill University
Montreal, Canada
Attn: Prof. G.A. Woonton, Director
The Eaton Electronics Research Lab.

Georgia Technical Research Inst.
Engineering and Experiment Station
722 Cherry Street, N. W.
Atlanta, Georgia
Attn: Dr. James E. Boyd

The University of Texas
Defense Research Laboratory
Austin, Texas
Attn: Claude W. Horton
Physics Library

Director
Evans Signal Laboratory
Belmar, New Jersey
Attn: Mr. O. C. Woodyard

Airborne Instruments Laboratory, Inc.
Division of Cutler Hammer
Walt Whitman Road
Melville, L. I., New York
Attn: Dr. E. Fubini, Director
Research & Engineering Division

Bell Aircraft Corporation
Post Office Box 1
Buffalo 5, New York
Attn: Eunice P. Hazelton, Librarian

Lockheed Aircraft Corporation
California Division, P.O. Box 551
Burbank, California
Attn: Mr. H. Rempt

Ryan Aeronautical Company
2701 Harbor Drive
Lindbergh Field
San Diego 12, California
Attn: J. R. Giantvalley

Boeing Airplane Company
Aero Space Division
P. O. Box 3707
Seattle 24, Washington
Attn: R. R. Barber
Library Supervisor

Office of Naval Research (Code 427)
Department of the Navy
Washington 25, D. C.

California Institute of Technology
Jet Propulsion Laboratory
Pasadena 4, California
Via: District Chief, Attn:ORDEV-M
Los Angeles Ordnance District
55 S. Grand Avenue
Pasadena, California

Polytechnic Institute of Brooklyn
Microwave Research Institute
55 Johnson Street
Brooklyn, New York
Attn: Dr. Arthur A. Oliner [2]

The Pennsylvania State University
Department of Electrical Engineering
University Park, Pennsylvania

Purdue University
Department of Electrical Engineering
Lafayette, Indiana
Attn: Dr. Schultz

University of Tennessee
Ferris Hall
W. Cumberland Avenue
Knoxville 16, Tennessee

Dr. U. Unz
University of Kansas
Electrical Engineergin Department
Lawrence, Kansas

Ohio State University Research Foundation
Antenna Laboratory
Attn: Dr. C. H. Walter
1314 Kinnear Road
Columbus 12, Ohio

Case Institute of Technology
Cleveland, Ohio
Attn: Prof. S. Seeley

New York University
Institute of Mathematical Sciences
25 Waverly Place, Room 802
New York 3, New York
Attn: Prof. Morris Kline

The University of Michigan
Engineering Research Institute
Willow Run Labs., Attn: Librarian
Willow Run Airport
Ypsilanti, Michigan

---

*One copy, unless otherwise specified by numbers enclosed in brackets.

Electronics Research Directorate Air Force Cambridge Research Labs. Office of Aerospace Research, USAF Bedford, Mass., Rpt. No. AFCRL63-90 THEORETICAL AND EXPERIMENTAL STUDIES OF ANTENNAS AND ARRAYS IN A PARALLEL-PLATE REGION:PART I, THE CURRENT DISTRIBUTION AND INPEDANCE OF AN ANTENNA IN A PARALLEL-PLATE REGION. Interim Scientific Rpt. No. 15(Series2), 5 October 1962, 66pp., illus., tables, 27 refs. -Presented at the URSI-IRE Fall Meeting, Ottawa, Canada, October, 1962. Unclassified Report	1. Antennas and components I. AF Project 5635 Task 563502 II. Contract AF19 (604)-4118 III. Cruft Laboratory Harvard U. Cambridge, Mass. IV. B. Rama Rao V. Sci Rpt. No. 15 (Series 2) VI. VII. In ASTIA collection

Closed form expressions for the current distribution and impedance of an antenna in a parallel-plate region have been obtained by an integral equation technique. Interesting features connected with the antenna are (1) the logarithmic singularity in the current near the driving point because of the idealized delta-function generator (2) behavior at resonance. The theoretical results have been verified experimentally and a description of the apparatus is included in the report.